(1) Cover page

Annual Technical Report

Title: Unraveling the nature of chemical reactivity of complex systems

Principal Investigator(s): Kopin Liu

Contract Number: FA4869-08-1-0006

AFOSR/AOARD Reference Number: AOARD-074005

AFOSR/AOARD Program Manager: Thomas E. Erstfeld

Period of Performance: 15 JAN 2008 – 14 JAN 2009

Submission Date: 13 JAN 2009

PI: Kopin Liu / Institute of Atomic and Molecular Sciences

Report Documentation Page

Form Approved
OMB No. 0704-0188

1. REPORT DATE	2. REPORT TYPE	3. DATES COVERED
14 JAN 2009	**Final**	**15-01-2008 to 15-01-2009**

4. TITLE AND SUBTITLE	5a. CONTRACT NUMBER
Unraveling the Nature of Chemical Reactivity of Complex Systems	**FA48690810006**
	5b. GRANT NUMBER
	5c. PROGRAM ELEMENT NUMBER
6. AUTHOR(S)	5d. PROJECT NUMBER
Kopin Liu	5e. TASK NUMBER
	5f. WORK UNIT NUMBER
7. PERFORMING ORGANIZATION NAME(S) AND ADDRESS(ES)	8. PERFORMING ORGANIZATION REPORT NUMBER
Institute of Atomic and Molecular Sciences,PO Box 23-166 Academia Sinica,Taipei, Taiwan,NA,10617	**N/A**
9. SPONSORING/MONITORING AGENCY NAME(S) AND ADDRESS(ES)	10. SPONSOR/MONITOR'S ACRONYM(S)
AOARD, UNIT 45002, APO, AP, 96337-5002	**AOARD**
	11. SPONSOR/MONITOR'S REPORT NUMBER(S)
	AOARD-074005

12. DISTRIBUTION/AVAILABILITY STATEMENT

Approved for public release; distribution unlimited

13. SUPPLEMENTARY NOTES

14. ABSTRACT

This project was to gain fundamental understanding of the chemical reactivity of complex systems, specifically the state-correlation of product pairs in chemical reactions of polyatomic molecules, and the salvation dynamics of ion-solvent interactions that are fundamental to many important phenomena in chemistry and biology.

15. SUBJECT TERMS

16. SECURITY CLASSIFICATION OF:			17. LIMITATION OF ABSTRACT	18. NUMBER OF PAGES	19a. NAME OF RESPONSIBLE PERSON
a. REPORT	b. ABSTRACT	c. THIS PAGE			
unclassified	**unclassified**	**unclassified**	**Same as Report (SAR)**	**33**	

(2) Objectives

The aim of this proposal is gain fundamental understanding of the chemical reactivity of complex systems. Specifically, the proposal consists of two experimental projects: (i) the state-correlation of product pairs in chemical reactions of polyatomic molecules, and (ii) the solvation dynamics in water clusters and in aqueous solution, in particular the ion-solvent interactions that are fundamental to many important phenomena in chemistry and biology.

(3) Status of the efforts

The crossed molecular beam project is an established one in this laboratory. In 2008 we took the full advantage of our unique capability of measuring the product pair correlation and continued making significant contributions to the field of chemical reaction dynamics, as evidenced from the invitations to write an article to Proc. Nat'l Acad. Sci. USA and to several international conferences as a plenary speaker.

The solvation dynamics is a new project funded mainly by Academia Sinica from 2008. Several initial tasks were carried out, including modifications of an existing apparatus for water cluster generation, the purchase of a state-of-the-art femtosecond laser system, and the installation of a clean-room facility to accommodate the new laser system etc. Those time-consuming preparation-phase works are mostly completed by the end of 2008.

(4) Abstract

We continued the fundamental study of the reactivity of Cl-atom towards methane. Being a competing reaction to Cl + O_3 and one of the major sinks for CH_4 (a greenhouse gas), this reaction plays a crucial role in atmospheric chemistry and is highly relevant to the ozone production/depletion problems. Our aim is to understand how different forms of reagent energy (translation and vibration) affect the reaction rate and detail dynamics. Following our earlier studies on Cl + CHD_3(v_1=1) and Cl + CH_4(v_3=1), we now extend to Cl + CH_2D_2(v_1=1 and v_6=1). Here, v_1=1 and v_6=1 indicate one-quantum excitation of the CH_2-symmetric stretching and CH_2-antisymmetric stretching mode of the CH_2D_2 reagent, respectively. These two modes are nearly degenerate, but with very different vibrational motions. Because the oscillation strengths of both IR-transitions are relatively weak, the experimental challenge is to pump up as much CH_2D_2 molecules as possible into the desired vibration mode. To this end, we have designed and fabricated a multipass ring reflector (Rev. Sci. Instrum. 79, 033105 (2008)) that effectively increases the infrared laser power by 10 folds, thus making the experiments feasible. Preliminary

analysis of the data reveals some very exciting results, which could drastically shape our thinking about mode- and bond-selective chemistry in the future.

In the other project aimed to understand the solvation dynamics of aqueous solution, some preparatory progresses have also been made. This is a new project funded by a very competitive 5-year Academia Sinica Investigator Award, starting from 2008. The major parts of a state-of-the-art femtosecond laser system have been purchased and just arrived. In order to accommodate the new laser system, the whole machine was shut down and a clear-room unit installed. We are now in the process of re-installing the machine and integrating it with the new laser system.

(5) Personnel Supported

Dr. J. Riedel (left for Fritz-Haber Institute of Berlin as a junior fellow)

Dr. H. Kawamata

Dr. S. Tauro

Mr. Y.-T. Wu (left for University of Virginia, USA, as a Ph. D. student)

Mr. Y.-J. Lu

Mr. J.-S. Chen

Mr. Gautam Sarma (an exchange student from University of Nijmegen, The Netherlands; Sept.- Dec. 2008)

(6) Publications

1. "Tracking the Energy Flow along the Reaction Path", S. Yan, Y.-T. Wu, and K. Liu, *Proc. Natl. Acad. Sci. USA* **105**, 12667 (2008). **(An invited article).**
2. "Anisotropies of Photoelectron Angular Distribution in the Vicinity of Autoionization resonances", S. Tauro and K. Liu, *J. Phys. B: At. Mol. & Opt. Phys.* **41**, 225001 (2008).
3. "Pair-Correlated Dynamics of the Reaction of Chlorine Atom with Antisymmetric Stretch-Excited Methane", H. Kawamata, S. Tauro, and K. Liu, *Phys. Chem. Chem. Phys.* **10**, 4378 (2008). **(The cover article).**
4. "Imaging the Dynamics and Isotope Effects of the Cl + CH_2D_2 Reaction" Y.-T. Wu and K. Liu, *J. Chem. Phys.* **129**, 154302 (2008).

(7) Interactions:

(a) Invited talks at International Conferences (* denoting plenary lectures)

1. "The 235th ACS National Meeting", New Orleans, LA, USA, April 4-10, 2008.

*2. "The 24th Symposium on Chemical Reaction Dynamics", Sapporo, Japan, June 2-4, 2008.

*3. "The 17th European Conference on Molecular Dynamics, MOLEC XVII", St. Petersburg, Russia, Aug. 23-28, 2008.

*4. "The 12th Stereodynamics of Chemical Reactions", Dalian, China, Oct. 13-18, 2008.

*5. "The 8th Asian International Seminar on Atomic and Molecular Physics, AISAMP8", Perth, Western Australia, Nov. 24-28, 2008.

Workshop organized

"Frontiers in Physical Chemistry: A Workshop for Students", Taipei, Taiwan, Oct. 20, 2008. [The six lecturers include three invited foreign scholars: Prof. David Nesbitt from JILA/University of Colorado, Prof. Andrew Orr-Ewing from University of Bristol, UK, and Prof. Steve Stolte from Free University, The Netherlands.]

International Collaborations

In collaboration with Professor Hans ter Meulen and Professor David Parker, both are at University of Nijmegen of The Netherlands, a Ph.D. student Mr. Gautam Sarma spent three months (Sept.- Dec. 2008) here to learn the know-how of product-pair correlation measurements.

(8) New

(a) List discoveries, inventions, or patent disclosures.

(None)

(9) Honors/Awards

(None)

(10) Archival Documentation

[The four publications listed in (6) are sent along with this report as the attached files.]

Tracking the energy flow along the reaction path

Shannon Yan*, Yen-Tien Wu, and Kopin Liu†

Institute of Atomic and Molecular Sciences, Academia Sinica, P.O. Box 23-166, Taipei 10617, Taiwan

Edited by F. Fleming Crim, University of Wisconsin, Madison, WI, and approved May 19, 2008 (Received for review January 8, 2008.

We report a comprehensive study of the quantum-state correlation property of product pairs from reactions of chlorine atoms with both the ground-state and the CH stretch-excited CHD_3. In light of available *ab initio* theoretical results, this set of experimental data provides a conceptual framework to visualize the energy-flow pattern along the reaction path, to classify the activity of different vibrational modes in a reactive encounter, to gain deeper insight into the concept of vibrational adiabaticity, and to elucidate the intermode coupling in the transition-state region. This exploratory approach not only opens up an avenue to understand polyatomic reaction dynamics, even for motions at the molecular level in the fleeting transition-state region, but it also leads to a generalization of Polanyi's rules to reactions involving a polyatomic molecule.

mode-specific chemistry | Polanyi's rules | product pair correlation

One of the central concepts in understanding chemical reactivity is the idea of the transition state (1). When two reactants collide to form reaction products, old bonds are broken and new bonds formed. This bond breaking and forming process must then occur over a molecular configuration intermediate between reactants and products, and this intermediate region of potential energy landscape is what chemists refer to as the transition state. The transition state is often located near the top of a potential barrier and acts as a bottleneck in a chemical reaction. The properties of the transition state therefore determine the reaction rate, as well as many of the more detailed observables from scattering experiments.

Over the past decades, there has been tremendous progress in experimental characterization of the structure of the transition state, notably by using the spectroscopic probes (2–4). Transition-state spectroscopy experiments performed to date are essentially the half-collision type in which the transition state is directly accessed either through photodetachment of negative ion precursor in a frequency-resolved experiment (3) or by the femtosecond pump-probe, time-resolved approach (4). As elegant and informative as those experiments are, half-collision results, in general, do not depict a full picture of how the reactants transform into the products. One way to think of this is as follows. The basic idea of a typical half-collision experiment is to initiate the reaction at transition state by a photoexcitation process. By virtue of photoabsorption, the total angular momentum, that is, the partial wave or the impact parameter, of the reactive system is then well specified and often limited to the lowest few quantum numbers in a restricted geometry of the Franck–Condon region. Consequently, the half-collision results are greatly simplified and more amenable to theoretical tests. In contrast, a chemical reaction inevitably constitutes the contribution from collisions with a full range of impact parameters and orientations. The resultant wave-interference patterns, arising from the coherent sum of scattering amplitudes of many partial waves, are manifested in the full-collision attribute such as product angular distribution (5, 6), which cannot be readily accounted for by the few-partial-wave, half-collision approach. On the horns of a dilemma, a full-collision experiment usually deals with asymptotic properties of the reaction, thereby rendering direct probes of the fleeting transition state difficult.

Here, we propose an approach to delineate the dynamical aspects of the transition state in a full-collision experiment by tracking the energy flow along the reaction path. We previously introduced an experimental method to unfold the state-specific correlation of coincident product pairs in polyatomic reactions (7–9). More recently, we exploited the product pair-correlation approach to elucidate mode-selective chemistry of the Cl + $CHD_3(v_1 = 1 \text{ or } v_3 = 1) \rightarrow HCl + CD_3(v = 0)$ reaction (10). In the latter study, we found that, contrary to the current perception, C–H stretch (v_1) excitation is no more efficient than an equivalent amount of translational energy in enhancing the reaction rate; CD_3 bend (v_3) excitation is only moderately more efficient. These unexpected results then raised an important question: How do we understand the observed differential reactivity between polyatomic reactant vibration and translation from the perspective of Polanyi's rules (11, 12)? The work reported here presents an all-important complement to resolve the apparent paradox by mapping out the complete energy-flow pattern through correlating as many coincidently formed product pairs as possible to an initially prepared reactant state. What emerged is a conceptually appealing picture in which the cooperative motion of atoms in passing through the transition state can be visualized. In addition, this conceptual framework leads naturally to a generalization of Polanyi's rules to a reaction involving polyatomic molecules.

What Are Polanyi's Rules?

Simply stated, Polanyi's rules concern how the barrier location influences the energy requirement and the energy disposal in a direct atom + diatom chemical reaction (11, 12). For an exothermic A + BC reaction, the reaction barrier is usually located in the entrance valley of the reaction, that is, an early barrier. According to Polanyi's rules, reactant translational energy is then more effective than vibration to surmount the barrier to reaction, thus, accelerating the reaction rate. The converse will be true for an endothermic, late-barrier reaction. By the principle of microscopic reversibility (1), the total available energy will then be deposited mostly into product vibration for an early-barrier reaction, whereas a translationally hot product will be yielded from a late-barrier reaction. Hence, the rule elucidates the role of different forms of energy (vibration versus translation) in an elementary chemical reaction, and links its intimate relationship to the underlying feature (the barrier location) of the three-atom interaction potential.

Experiment on Product Pair-Correlated Images

We performed the experiment under single-collision conditions by using a crossed molecular beam apparatus (7, 10, 13, 14). A discharge-generated, pulsed Cl beam (5% Cl_2 seeded in He at 6 atm total pressure) was double-skimmed and directed to cross with a pulsed CHD_3 molecular beam in a high-vacuum chamber. A tunable infrared (IR) optical parametric oscillator/amplifier

Author contributions: K.L. designed research; S.Y. and Y.-T.W. performed research; S.Y. and Y.-T.W. analyzed data; and K.L. wrote the paper.

The authors declare no conflict of interest.

This article is a PNAS Direct Submission.

*Present address: Department of Chemistry, University of California, Berkeley, CA 94720.

†To whom correspondence should be addressed. E-mail: kliu@po.iams.sinica.edu.tw.

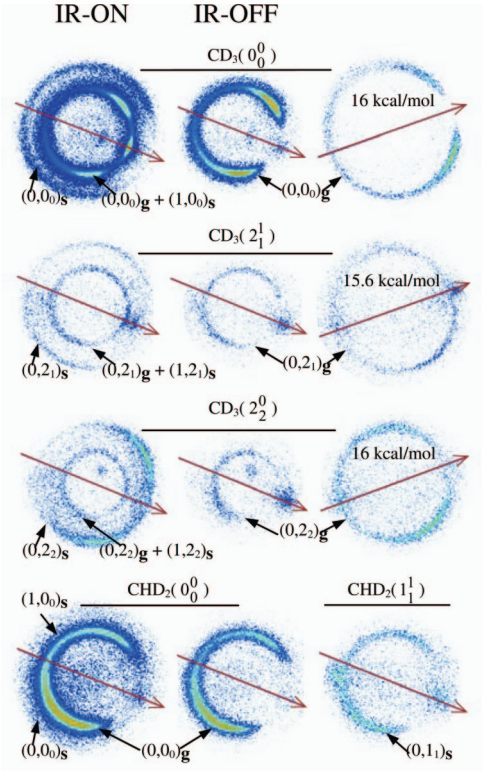

Fig. 1. Raw images, with (*Left*) and without (*Center*) IR-pumping, of probed product states from the Cl + CHD_3 reaction at E_c = 8.1 kcal/mol. REMPI bands used to probe the methyl products are indicated in parentheses. For $CHD_2(1^1_1)$ no detectable signals can be observed from the IR-off image. Also exemplified for the CD_3 states are the three IR-off images acquired at E_c ≈16 kcal/mol (*Right*), that is, with approximately the same total energy as the C–H stretch-excited reactant at E_c = 8.1 kcal/mol. Because of the weak signals, some backgrounds (appearing as blurred spots) were observed but discarded in data analysis. The ringlike feature can be ascribed, on energetic grounds, to the product-state pair as labeled (see text for notations).

prepared the CHD_3 reactant, before the collision center, with one-quantum excitation along the C–H stretching bond via the $v_1 = 0 \rightarrow 1$, R(1) transition at 3,005.57 cm^{-1} (15). After the collision, the reaction products, either CD_3 or CHD_2 radicals, were probed by (2 + 1) resonance-enhanced multiphoton ionization (REMPI) spectroscopy ≈331–339 nm depending on the REMPI bands (16–18), and a time-sliced ion velocity imaging technique mapped the state correlation of coincidently formed coproducts HCl or DCl (7–9). (Under the experimental conditions of this study, the estimated scaling (up) factors for probing the 2_1, 2_2, and 2_3 states of CD_3 radical are 9.0 ± 0.5, 3.5 ± 0.5, and 16.4 ± 2.0, respectively. The notation of 2_i refers to the vibrational mode 2 (the umbrella-bend) with i-quantum excitation.) Pair-correlated state and angular distributions were then exploited, in light of available *ab initio* theory (19–22), to unveil the microscopic reaction pathways. We further sharpened the comparison with the result of a ground-state reaction at either the same initial translation energy (E_c) or the higher E_c with an equivalent amount of total energy (vibration + translation).

Fig. 1 presents several raw images with the probe laser frequencies fixed at the peak of the Q branch of the respective REMPI bands. The vibronic band notation in the figure is such that 2^1_1 designates the spectroscopic transition involving the v_2 (umbrella-bend) mode with one-quantum excitation each in both the electronically ground state (the subscript) and the electronically excited state (the superscript). Methyl product state was probed with the IR-excitation on and off in an alternative manner. Very small signals from the C–H stretch-excited reaction were also detected for one-quantum excitation in the v_4 (in-plane bend) and the v_3 (antisymmetric stretch) modes of the CD_3 product, but they were too weak to be quantified. No other CD_3 or CHD_2 modes showed detectable signature from the C–H stretch-excited reaction, although some of them indicated very weak signals from the ground-state reaction. It is quite remarkable that, despite numerous product states being energetically accessible, so few product vibrational modes are active in this reaction. Typical signals for vibrationally excited methyl products shown in Fig. 1 were only a few percent of that for the ground-state product. In addition to the less favorable REMPI-detection sensitivity when probing the vibrationally excited products than the 0^0_0 origin band (16), the loss in signals from the C–H stretch-excited reaction also arises from the fact that only ≈20% of reactants were excited by the IR laser (10, 13, 14).

The energetics of the reaction are well defined: the reaction endothermicities are 1.73 and 1.94 kcal/mol for the H and D atom abstraction channels, respectively. E_c was kept ≈8.1 kcal/mol and the initial ro-vibration excitation of $CHD_3(v_1 = 1, j = 2)$ adds another 8.63 kcal/mol to the total energy. (The K quantum number of CHD_3 was not resolved in this study.) By conservation of energy and momentum, the maximum velocities of the coproduct HCl (or DCl), recoiling from the state-selected CD_3 (or CHD_2), in different vibration states were calculated and identified as the ringlike features on images in Fig. 1. The clear separation between the rings indicates unequivocally the low rotational excitation of the HCl (or DCl) coproduct. The relative intensity of the ring on a given image reflects the probability for the coincident formation of the corresponding HCl or DCl state. The intensity around each ring then gives an immediate impression about the preferred scattering direction of the product state. [Superimposed on each image in Fig. 1 is a red arrow, pointing to the 0^0-angle that is defined as the direction (in the center-of-mass frame) of the initial CHD_3 beam.] Inspection of the image reveals rich variations not only among different methyl product states, but also for a given state under the three different experimental conditions.

Such variations are better appreciated, after data analysis, in terms of the pair-correlated vibration branching and angular distribution (7, 8). As indicated in Fig. 1, the inner ring on each of the three CD_3 IR-on images (*Left*, top three) constitutes two nearly degenerate components. (Recall that the vibrational energy of stretch-excited reactants is 8.63 kcal/mol and the formation of $HCl(v' = 1)$ requires at least 8.24 kcal/mol.) A forward ringlike feature that is absent on the IR-off image (Fig. 1 *Center*) corresponds to the concomitantly formed $HCl(v' = 1)$ from the stretch-excited reaction. In the side- and back-scattering directions, however, the signal of this product pair overlaps with the contribution of the $HCl(v' = 0)$ pair from the ground-state reactants that are unpumped by the IR laser. To disentangle the pair-correlated angular distribution of the stretch-excited reaction from the IR-on image, the fraction of C–H stretch-excited reactants (typically ≈20%) in the CHD_3 beam was first determined by the threshold method (13). By scaling down the IR-off angular distribution by 0.20 to account for the unpumped ground state CHD_3 and subtracting it from the IR-on data, the genuine distribution from the stretch-excited reaction was then uncovered from the overlapped ringlike feature. The results of such analysis, along with those for the outer rings, are summarized in Fig. 2.

For the Cl + $CHD_3(v_1 = 1) \rightarrow HCl(v') + CD_3(v_i)$ reaction, all three product pairs associated with $HCl(v' = 1)$ display a similar angular pattern (Fig. 2*A*): a sharp forward peak superimposed on a nearly isotropic component. The sharpness of the forward peak, however, descends in the order of $(1, 0_0)_s > (1, 2_1)_s > (1, 2_2)_s$. Here, the product-state pair is labeled as follows: the

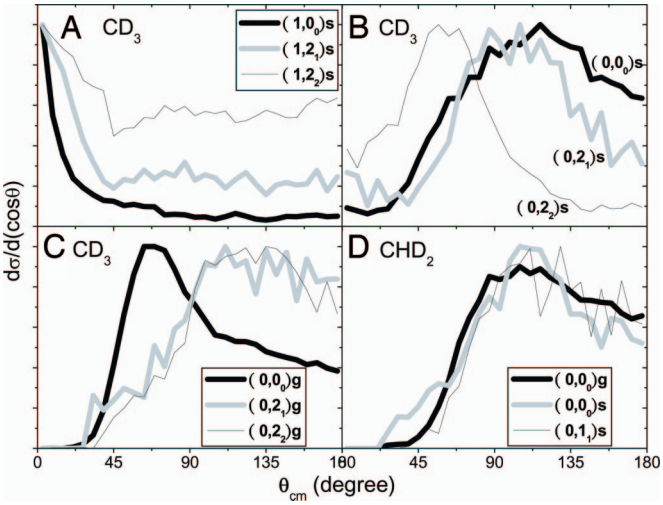

Fig. 2. Summary of the state-correlated angular distributions at E_c = 8.1 kcal/mol. The distributions for the ground-state reaction at E_c = 16 kcal/mol shift more forward as anticipated (10, 24, 25), thus not shown here. To contrast the variation in shapes, the angular distributions in each panel are plotted with approximately the same peak heights.

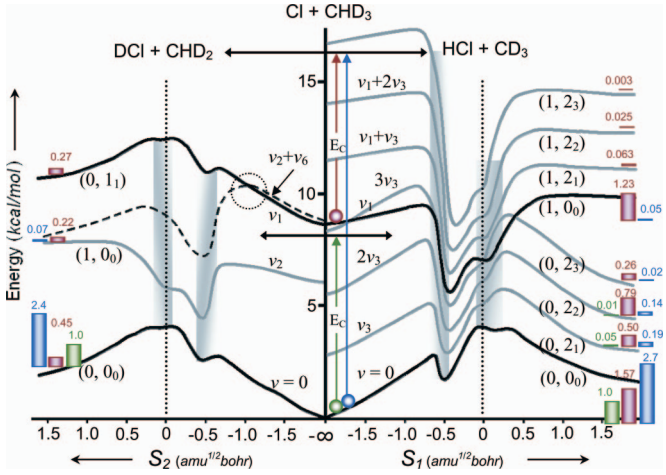

Fig. 3. Schematic representation of vibrationally adiabatic potential energy curves along the reaction coordinate *S*. (*Right*, left-hand side) The HCl + CD_3 (DCl + CHD_2) isotope channel. For clarity, only those states relevant to this study are shown. The shaded areas (near S = 0 and −0.5 $amu^{1/2}$bohr) denote the regions of strong curvature and Coriolis couplings, where vibrationally nonadiabatic transitions occur. For the HCl + CD_3 isotope channel, the relative cross-sections of different product-state pairs under three different experimental conditions are normalized and represented by the colored bars; those for the DCl + CHD_2 product channel are normalized independently. The color codes are: green and blue, ground-state reactions at E_c = 8.1 and 16 kcal/mol, respectively; red, the stretch-excited reaction at 8.1 kcal/mol. The estimated uncertainties associated with each number are ±10%, ±15%, and ±15% for the 2_1, 2_2, and 2_3 pairs, respectively.

numbers in the parentheses denote (from left to right) the quanta of vibrational excitation in HCl and the mode (v_i) in CD_3 products, respectively; the inner subscript specifies the quantum of CD_3 mode and the outer subscript indicates the ground (g) or the stretch-excited (s) reactant states. Angular distributions for the product pairs associated with HCl($v' = 0$) from the stretch-excited reaction, Fig. 2*B*, display rather different patterns: Both $(0, 0_0)_s$ and $(0, 2_1)_s$ pairs show predominantly backward-sideways distributions, whereas the $(0, 2_2)_s$ pair indicates a significant forward preference.

For the ground-state reaction (Fig. 2*C*), the angular distribution of the $(0, 0_0)_g$ pair displays a characteristic sideways peak accompanied by a sharp cutoff against forward scattering, indicative of a direct reaction mechanism governed by large impact-parameter collisions, that is, peripheral dynamics (23–25). The distributions for $(0, 2_1)_g$ and $(0, 2_2)_g$ also exhibit the sharp forward cutoff, albeit more backscattered, suggesting a direct rebound mechanism with significantly more contributions from smaller impact-parameter collisions than the $(0, 0_0)_g$ pair. This trend corroborates well with the chemical intuition that for a collinear Cl–H–C transition state, the smaller impact-parameter collisions will preferentially lead to the umbrella-excited CD_3 products. Comparing Fig. 2 *B* and *C*, the formation of some scattered products near the 0^0-angle for the $(0, 0_0)_s$, $(0, 2_1)_s$, and $(0, 2_2)_s$ pairs (Fig. 2*B*) is particularly noteworthy (see below). Aside from these forward-scattered features, it is intriguing to note that the global shapes of the angular distributions for $(0, 0_0)_s$ and $(0, 2_1)_s$ resemble those for $(0, 2_1)_g$ and $(0, 2_2)_g$, whereas the distributions for $(0, 2_2)_s$ and $(0, 0_0)_g$ seem alike in appearance.

As to the DCl + CHD_2 isotope channel (Fig. 2*D*), the observed angular distributions for all product pairs from either the ground-state or the CH stretch-excited reactant are virtually identical. The dominance of side- and back-scattered products is reminiscent of typical direct abstraction reaction governed by rebound mechanism (1).

Visualizing the Cooperative Atomic Motions While a Chemical Reaction Is Taking Place

The Conceptual Framework. To shed more light on the dynamics underlying the intricate angular pattern, we examined the relative branching ratio of the product-state pair. In deriving the branching ratio of each pair, we normalized its flux to the $(0, 0_0)_g$ pair from the ground-state reaction at E_c = 8.1 kcal/mol. Both the fraction of stretch-excited reactants (≈20% of total) and the different detection sensitivity when probing the excited CD_3 products (16) were taken into account in the HCl + CD_3 channel. Relative sensitivities of detecting CHD_2($v = 0$ and $v_1 = 1$) are yet to be calibrated; thus, their normalizations are just based on signal strengths and are independent of the HCl + CD_3 channel. The final results are summarized in Fig. 3, along with the adiabatic correlation of the relevant vibrational energy levels leading to both isotopic product channels.

By using the reaction path Hamiltonian approach (26), previous *ab initio* calculations of isotopically analogous reactions mapped out the minimum energy path and the evolution of the vibrational frequencies of various modes along the reaction path (19–22). By adding the theoretically calculated vibration frequencies (with isotope corrections) to the minimum energy path, we connected the vibrational energy levels according to their symmetries, employing the rule that energy levels for vibration of the same symmetry do not cross (26).

Theory predicted that as the Cl atom approaches the H end of CHD_3, the chemical interaction induces a static curvature coupling (i.e., coupling of a vibrational mode to the reaction coordinate induced by the curvature of the reaction path) between the C–H stretching (v_1) motion and the reaction coordinate, resulting in a significant decrease of its frequency in the transition-state region (19–22) and allowing energy flow between this mode and the reaction coordinate. Similar behavior was found for the CD_3 umbrella mode (v_3), yet other modes show little variation in frequencies. Theoretical calculations further predicted that these two active vibrations (v_1 and v_3) significantly couple to each other via Coriolis interactions (21), that is, the intermode mixings induced by the twisting of the two transverse vibrations about the curved reaction path as the reaction proceeds. Both curvature and Coriolis couplings are particularly strong near the shaded regions in Fig. 3. As the Cl atom

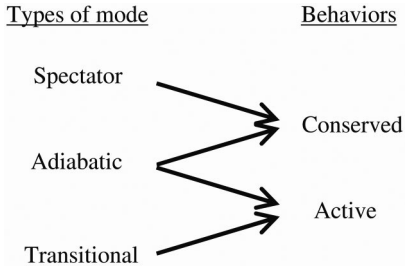

Fig. 4. Classification of the activity of reactant vibrational modes in a chemical reaction. By using the present reaction for illustration, an example of the spectator mode is the C–H stretching excitation in the Cl + $CHD_3(v_1 = 1) \rightarrow DCl(v' = 0) + CHD_2(v_1 = 1)$ channel, and of the adiabatic mode in the Cl + $CHD_3(v_1 = 1) \rightarrow HCl(v' = 1) + CD_3(v = 0)$ channel. The bend-excited CHD_3 behaves as a transitional mode in the Cl + $CHD_3(v_3$ and/or $v_6 = 1) \rightarrow HCl(v' = 0) + CD_3(v = 0)$ reaction.

approaches the D atom, however, the CD_3 symmetric stretch (v_2) is now brought to couple to the reaction coordinate (19). Near the transition state, it mixes extensively with the umbrella mode (v_3), the CD_3 rock (v_6), and possibly the CD_3 deformation (v_5) mode. In contrast, the C–H stretching frequency now becomes invariant, in accord with the chemical intuition that the nonreacting C–H bond behaves as a *spectator* when the Cl atom attacks the D end of CHD_3.

Fig. 3 is, of course, merely the vibrational correlation diagram. Vibrational motion rarely behaves entirely adiabatically during the course of a chemical reaction. Moreover, in analogy to the electronic Bohn–Oppenheimer approximation (1), the concept of vibrational adiabaticity is rooted on the relative time scales of the vibrational period and the interaction time. Although the latter is governed by the "slow" motion of the two heavy reactants in the present reaction, the adiabatic concept could become blurred for the low-frequency modes. Keeping this in mind and allowing for vibrational nonadiabaticity, Fig. 3 serves as our starting point for visualizing, at least in a qualitative sense, the energy flow while bond breaking and bond formation are taking place.

To make the concept more concrete and to set the stage for further discussion, Fig. 4 classifies the limiting behaviors of different vibrational modes in a chemical reaction. Reactant vibration is called *conserved* if it is retained as one of the vibrational motions of the product. During the reaction, it can either remain as a *spectator* (i.e., preserving its mode character with the vibrational frequency nearly unchanged throughout the reaction path) or behave *adiabatically* (i.e., preserving the vibrational quantum number but with varying frequencies due to the static curvature coupling to the reaction coordinate). In the former case, vibrational excitation in the nonreactive bond (spectator) does not actively participate in the reaction; thus, the initial excitation in that bond is likely to be retained in the final product vibrational distribution. In the adiabatic case, energy exchanges between the vibration and the motion along the reaction coordinate can occur; thus, an adiabatic vibration is an *active* participant in the reaction. Another type of active mode is the *transitional* vibration (27), for which the vibrational motion of the reactant, usually of a low-frequency mode, does not correlate to any product vibration, rather it evolves into the rotation and translation of the departing products.

In general, the activity of a reactant vibrational mode will fall into at least one of the above types: spectator, adiabatic, and transitional. Although a spectator (transitional) mode is always conserved (active), the adiabatic mode can partake in both behaviors in a reaction. It should also be pointed out that the classification here refers to the limiting cases and is not always unambiguous. A given mode may change its activity from one type to the other along the reaction path due to the curvature and intermode Coriolis couplings. Consequently, the occurrence of bifurcating reactive fluxes into multiple microscopic reaction paths may well be a norm rather than an exception.

As the Cl Atom Abstracts the Stretch-Excited H Atom. A recent study on the ground-state Cl + CHD_3 reaction demonstrated that nearly 98% of products were the ground-state pair $(0, 0_0)_g$ when $CD_3(v = 0)$ was probed (10); a similar result was obtained for Cl + CH_4 (25). Detailed analysis of the IR-off images (Fig. 1) revealed that the relative branching ratios of the $(0, 2_1)_g$ and $(0, 2_2)_g$ pairs to $(0, 0_0)_g$ at $E_c = 8.1$ kcal/mol (Fig. 3, green bars) are merely 0.05 and 0.01, respectively, which increase slightly to 0.07 (or 0.19/2.7) and 0.05 (or 0.14/2.7) even at $E_c = 16$ kcal/mol (Fig. 3, blue bars). The ground-state reaction is therefore, by and large, vibrationally adiabatic. Previous experiments on reactions with umbrella-excited CHD_3 (10) or CH_4 (28) demonstrated the dominance of the $(0, 0_0)_b$ product pair; its angular distribution is almost identical to that from the ground-state reaction at the same E_c, suggesting instead a predominantly nonadiabatic pathway. In other words, because of the strong curvature coupling in the entrance valley, the umbrella-bending vibration of methane actually behaves as a transitional mode rather than as an adiabatic mode that would have yielded the $(0, 2_1)_b$ product pair by vibrational correlation.

For the C–H stretch-excited reactant, the reaction proceeds initially over the $v_1 = 1$ potential energy surface at long range. As the intermolecular distance decreases, a (avoided) crossing of the $v_1 = 1$ and $v_3 = 3$ (labeled as $3v_3$ in Fig. 3) adiabatic curves in the entrance valley could mix in some CD_3 umbrella-bending character into the C–H stretching motion. Around $S_1 \sim -0.5$ $amu^{1/2}bohr$, strong curvature couplings take place, resulting in a bifurcation of reactive trajectories into a vibrationally nonadiabatic as well as the adiabatic pathways. As can be envisioned from Fig. 3, energy flowing out of the initially deposited C–H stretch will be greatly facilitated, via Coriolis couplings, by the proximate umbrella-excited energy surfaces near the shaded regions. Compared with the branching ratios for $(0, 2_1)_g$ and $(0, 2_2)_g$ from the ground-state reaction (Fig. 3, green or blue bars), the analogous product pairs from the C–H stretch-excited reaction (Fig. 3, red bars) show significantly larger ratios, in support of this interpretation. In conjunction with the strong curvature couplings of both (stretching and umbrella-excited) active modes to the reaction coordinate (19–22), a cascading energy flow could lead to a higher population in the ground-state pair $(0, 0_0)_s$ than the $(0, 2_i)_s$ pairs, which is exactly shown in Fig. 3.

The above nonadiabatic reaction path is a direct mechanism, yet it is mediated by the umbrella motion and invokes a different reaction profile from the ground-state reaction. Observation of different angular distributions for the $(0, 0_0)_s$ and $(0, 0_0)_g$ pairs (Fig. 2) is therefore not too surprising. As to the v_2-excited product pairs $(0, 2_1)_s$ and $(0, 2_2)_s$ from the stretch-excited reaction, additional pathways might also come into play (see below). Nonetheless, the striking contrast in the general appearance, as alluded to earlier, between the two sets of analogous pair-correlated angular distributions from the ground and stretch-excited reactant states (Fig. 2 *B* vs. *C*) is intriguing and calls for further theoretical work for deeper understanding.

Not all reactive trajectories undergo nonadiabatic transitions; those that remain vibrationally adiabatic will retain their original character in the sense that the one quantum of stretching excitation is preserved within the Cl–H–C moiety of the colliding pair. Those trajectories could be temporarily trapped by the dynamic well associated with the stretch-excited adiabatic curve in the transition state region (Fig. 3), allowing more time for energy redistribution (10, 25). Angular distributions for the $(1, 0_0)_s$, $(1, 2_1)_s$, and $(1, 2_2)_s$ product pairs (Fig. 2*A*) are distinct from the corresponding pairs with $HCl(v' = 0)$ products (Fig. 2*B*), showing a forward peak on top of an isotopic component—a

characteristic distribution for reaction involving a short-lived complex (6, 29–33). We assert that those products paired with HCl($v' = 1$) are produced predominantly from a complex-forming pathway, and conceivably are mediated through a resonance state trapped by the dynamic well (10, 25).

Further intracomplex energy redistribution might occur before the resonant complex decays adiabatically to the HCl($v' = 1$) product pairs. In particular, the proximity of the $(0, 2_2)$ curve near $S_1 \approx 0$ amu $^{1/2}$bohr suggests that it is a competing nonadiabatic path. The inverted branching ratios between $(0, 2_2)_s$ and $(0, 2_1)_s$, 0.79 vs. 0.50 (Fig. 3), support this view. The observation that the relative reactive fluxes in the forward direction (Fig. 2*B*), which could be regarded as the imprint of the vibrationally nonadiabatic decay of resonant complexes, decrease progressively in the order of $(0, 2_2)_s > (0, 2_1)_s > (0, 0_0)_s$ also closely corroborates this scenario. It is worth noting that from the branching ratios listed in Fig. 3, the excited HCl($v' = 1$) pairs from the C–H stretch-excited reaction (Fig. 3, red bars) collectively account for ≈30% of total reactivity of the HCl + CD_3 isotope channel. Treating it as a rough estimate of vibrational adiabaticity, the overall nonadiabatic pathways appear quite facile.

As the Cl Atom Attacks the Unexcited D Atoms. For the other isotope channel DCl + CHD_2, only three product pairs, $(0, 1_1)_s$, $(1, 0_0)_s$, and $(0, 0_0)_s$, are significantly populated from the C–H stretch-excited reactant. Theory predicts that the C–H stretching frequency hardly changes as the Cl atom attacks the D atoms (19), implying that the initial C–H excitation remains localized as a spectator in forming the adiabatically correlated product pair $(0, 1_1)_s$. And the shape of the C–H stretch-excited reaction path for forming the $(0, 1_1)_s$ pair should be nearly identical to that for producing the $(0, 0_0)_g$ pair from the ground-state reactant (Fig. 3). If the stretch-excited reaction indeed proceeds adiabatically, then the angular distribution of the $(0, 1_1)_s$ pair should be similar to the $(0, 0_0)_g$ distribution. That is exactly what we observed (Fig. 2*D*). Yet, the measured branching ratios (the red bars) showed significant variance with that from the ground-state reaction (either the green or blue bars). In particular, the adiabatically correlated $(0, 1_1)_s$ pair accounts for only 30% of total reactivity of this isotope channel (a value identical to the other isotope channel may be fortuitous), in significant deviation from the adiabatic expectation or the spectator paradigm (34, 35) that the initial excitation of the unreactive C–H bond survives as the $(0, 1_1)_s$ product pair. Therefore, the initial C–H excitation is counterintuitively not a mere spectator when a D atom is abstracted.

The angular distribution for the dominant $(0, 0_0)_s$ pair in the D atom abstraction channel is virtually identical to the other two pairs (Fig. 2*D*). The formation of the $(0, 0_0)_s$ pair, however, must involve a facile nonadiabatic pathway to funnel the energy initially deposited in the C–H bond into the rotational and translational motions of the departing products. What kind of cooperative nuclear motions might partake in redistributing the initially localized C–H stretching energy as the Cl atom is abstracting a D atom? Theoretical calculations suggested that the CD_3 symmetric stretch (ν_2) mode of CHD_3 is an active mode in this isotope channel (19). As depicted in Fig. 3, we conjectured that several proximate combination modes involving the ν_2 mode of CHD_3, for example, $\nu_2 + \nu_6$, are the plausible candidates for nonadiabatic transitions, as illustrated by the dashed circle, in the entrance valley. [The rocking vibration ν_6 is a transitional mode, which preferentially leads to the rotational and translational motions of reaction products (19).] The shape of the reaction path for $\nu_2 + \nu_6$ is uncertain because of the strong mixings between the ν_6 and ν_3/ν_5 modes in the transition-state region, thus, plotted as a dashed line in Fig. 3. Tentatively, the reaction starts with a C–H stretch-excited reactant in the entrance valley. Near the circled region, ≈30% of reactive fluxes stay adiabatic and eventually yield the $(0, 1_1)_s$ product pair; the other 70% of reactive fluxes make a nonadiabatic transition to the combination-mode-excited path. As the reaction proceeds further, extensive couplings occur around $S_2 \sim -0.5$ amu$^{1/2}$bohr and energy can flow into the other degrees of freedom. Approximately two-thirds, or 0.45/(0.45 + 0.22), end with the ground-state product pair through nonadiabatic processes, and one-third, or 0.22/(0.45 + 0.22), forms as the $(1, 0_0)_s$ pair.

Mode-Specific and Bond-Selective Reactivity

These issues are at the heart of polyatomic reactivity and have been actively pursued both experimentally (10, 28, 34–37) and theoretically (19–22) in recent years. We have reported a strong mode specificity in terms of pair-correlated distributions for two different modes of excitation: the C–H stretch and umbrella bend of the Cl + CHD_3 → HCl + CD_3 reaction (10). As presented above (Fig. 3, the colored bars), sharp contrasts on the pair-correlated branching ratios in both isotope channels are also noted when compared with the C–H stretch-excited and ground-state reactions. It is insightful here to have a global view of the total reactivity, that is, the sum of the pair-correlated branching ratios in each isotopic channel, under three different experimental conditions.

For the DCl + CHD_2 channel, the total reactivity of the ground-state reaction at $E_c = 8.1$ kcal/mol (Fig. 3, green bar), the C–H stretch-excited reaction at the same E_c (the sum of the red bars), and the ground-state reaction at 16 kcal/mol (the blue bars) are 1.0, 0.94, and 2.47, respectively. A total reactivity of 0.94 for the C–H stretch-excited reactant is not much different from the ground-state reactivity of 1.0 at the same E_c. In other words, although the initial one-quantum excitation of the C–H stretch (a spectator bond here) exerts enormous effects on product state distributions that deviate from the spectator picture because of the breakdown of vibrational adiabacity, it does not alter much the total reactivity of the D atom transfer channel. The latter conclusion seemly conforms to the spectator-bond paradigm that the vibrational energy in the nonreacting bond yields little effect on the reaction rate (34, 35). Hence, spectator or not depends on the measured quantity.

As to the HCl + CD_3 channel, the total reactivity of the ground-state reaction is 1.06 (the sum of the green bars) and 3.1 (the blue bars) at $E_c = 8.1$ and 16 kcal/mol, respectively; and the relative reactivity for the stretch-excited reactant at 8.1 kcal/mol becomes 4.44 (the red bars). Hence, with the equivalent amount of total energy, the stretching vibration is more effective than pure translation energy by a factor of ≈1.4 (or 4.44/3.1) in this isotope channel. This finding seems in accord with the expectation of Polanyi's rules, as well as with the chemical intuition that the vibrational energy is directly deposited into the bond (C–H) to be broken. However, the enhancement factor of 1.4 for a stretch-excited reactant is virtually the same as that obtained for a bend-excited reactant (10). Thus, the preferential promotion of total reactivity by vibration in the HCl + CD_3 channel does not appear to be mode-specific.

Moreover, when both isotope channels are considered, the combined enhancement factor by stretch-excitation, (4.44 + 0.94)/(1.06 + 1.0) = 2.61, turns out to be nearly the same as the translational enhancement of 2.7, that is, (3.1 + 2.47)/(1.06 + 1.0). In other words, vibration is no more efficient than translation in promoting the overall reactivity. These seemingly conflicting views about the reactant vibrational effects—more effective in one isotope channel but not in overall reactivity—stem from the different activities of the C–H stretch-excitation partaking in the two isotopic product channels: behaving as an adiabatic/transitional mode in the H atom abstraction channel and as a spectator/transitional mode when the D atom is transferred. Consequently, although the C–H stretching vibration is more effective than translation in promoting the formation of HCl + CD_3, the converse is true for the DCl + CHD_2 channel.

In terms of the overall isotopic product branching ratio $[HCl+CD_3]/[DCl+CHD_2]$, the stretch-excited reactant increases the ratio from 1.06 for ground-state reactant at $E_c = 8.1$ kcal/mol to 4.72 (or 4.44/0.94), which is to be compared with a value of 1.26 (or 3.1/2.47) for translationally hot ground-state reaction. This differential isotope effect between the stretch-excitation and translational energy, or the preferential cleavage of the excited C–H bond, is a manifestation of bond-selective chemistry (36, 37).

A Renaissance of Polanyi's Rules for Polyatomic Behavior

How do we reconcile the present viewpoint with the venerable Polanyi's rules (11, 12) that are taught in textbooks to understand the energy disposal and requirement in a direct atom + diatom reaction (1, 38)? Transition-state structure in an exothermic three-atom reaction is, in general, reactant-like according to Hammond's postulate (1); thus, an attractive surface or an early barrier is predicted by Polanyi's rules. Because the barrier is located in the entrance valley where the potential shape transverse to the reaction coordinate is not yet strongly perturbed by the intermolecular interactions, the (diatomic) reactant vibrational frequency should not alter significantly. Hence, from Fig. 4, the reactant vibration behaves as a *spectator* during motions up to the transition-state region, and little vibrational enhancement in reactivity is expected. However, for an endothermic A + BC reaction, the structure of the transition state will be product-like and the barrier lies late in the exit valley. As the reaction proceeds and before the transition state, the colliding pair must pass through the corner-cutting region where the vibrational frequency orthogonal to the minimum energy path changes because of the curvature coupling to the reaction coordinate, facilitating the energy exchange between the initial vibration excitation and the motion along the reaction coordinate. Therefore, the vibrational energy of reactant becomes effective in promoting reaction rate and yields translationally hot products. Reactant vibration is now *active* and often behaves as a *transitional* mode in reaction.

As one might surmise from the above, the premise behind our approach to extending Polanyi's rules to a polyatomic reaction is the recognition of different activities or responses of multiple vibrational modes toward the interacting atom (Fig. 4). Although the numbers of the vibrational modes with motions orthogonal to the reaction coordinate scale as 3N-7, which can be quite large as the size of molecule increases, possible types of their activities in a reaction may remain quite limited. (Taking the present 6-atom reaction as an example, the number of internal (or vibrational) degrees of freedom of the system evolves from 9 on the reactant side to 12 at the transition state, and to 7 for the two molecular products. During the course of chemical reaction, one of the 12 degrees of freedom near the transition state corresponds to the reaction coordinate and the other 11 modes are the vibrational motions orthogonal to the reaction path.) Illustrating in this report a prototypical $Cl + CHD_3$ reaction outlines our attempt to qualitatively comprehend the dominant factors that govern the polyatomic reactivity. Theoretically, we adopted the reaction path Hamiltonian approach, along with previous high-level *ab initio* calculations for an approximate yet illuminating elucidation of the mode activities and the intermode couplings to account for vibrational nonadiabaticity. Experimentally, product pair correlation was exploited to disentangle the intricate pathways at the vibrationally correlated level (Fig. 3). Putting them together, the cooperative nuclear motions during the course of a chemical reaction were qualitatively decoded and then unveiled. Depending on the motional response, different vibration modes will exhibit different mode- or bond-selective behaviors. Hence, within the conceptual framework proposed here, the "generalized" Polanyi's rules can be regarded as a ramification or the other side of the coin of mode-specific reactivity.

ACKNOWLEDGMENTS. We thank X. Yu for his assistance in some experiments. This work was supported in part by National Science Council of Taiwan, Academia Sinica, and the Air Force Office of Scientific Research (AOARD-07-4005).

1. Levine RD, Bernstein RB (1987) *Molecular Reaction Dynamics and Chemical Reactivity* (Oxford Univ Press, Oxford).
2. Polanyi JC, Zewail AH (1995) Direct observation of the transition state. *Acc Chem Res* 28:119–132.
3. Neumark DM (2002) Spectroscopy of reactive potential energy surfaces. *PhysChemComm* 5:76–81.
4. Zewail AH (2000) Femtochemistry: Atomic-scale dynamics of the chemical bond using ultrafast lasers. *Angew Chem Int Ed* 39:2586–2631.
5. Liu K (2001) Crossed-beam studies of neutral reactions: State-specific differential cross sections. *Annu Rev Phys Chem* 52:139–164.
6. Liu K (2006) Recent advances in crossed-beam studies of bimolecular reactions. *J Chem Phys* 125:132307.
7. Lin JJ, Zhou J, Shiu W, Liu K (2003) Application of time-sliced ion velocity imaging to crossed molecular beam experiments. *Rev Sci Instrum* 74:2495–2500.
8. Lin JJ, Zhou J, Shiu W, Liu K (2003) State-specific correlation of coincident product pairs in the $F + CD_4$ reaction. *Science* 300:966–969.
9. Liu K (2007) Product pair correlation in bimolecular reactions. *Phys Chem Chem Phys* 9:17–30.
10. Yan S, Wu YT, Zhang B, Yue X, Liu K (2007) Do vibrational excitations of CHD_3 preferentially promote reactivity toward the chlorine atom? *Science* 316:1723–1726.
11. Polanyi JC (1987) Some concepts in reaction dynamics. *Science* 236:680–690.
12. Polanyi JC (1972) Some concepts in reaction dynamics *Acc Chem Res* 5:161–168.
13. Yan S, Wu YT, Liu K (2007) Disentangling mode-specific reaction dynamics from overlapped images. *Phys Chem Chem Phys* 9:250–254.
14. Yan S, Liu K (2007) Pair-correlated dynamics of $Cl + CHD_3(v_1=1)$ reaction: Effects of probe laser frequency. *Chin J Chem Phys* 20:333–338.
15. Rea DG, Thompson HW (1956) Vibration-rotation bands of trideuteromethane. *Trans Faraday Soc* 52:1304–1309.
16. Zhou J, Lin JJ, Shiu W, Pu SC, Liu K (2003) Crossed-beam scattering of $F + CD_4 \rightarrow DF + CD_3(v\mathrm{NK})$: The integral cross sections. *J Chem Phys* 119:2538–2544.
17. Zhang B, Zhang J, Liu K (2005) Imaging the ''missing'' bands in the resonance-enhanced multiphoton ionization detection of methyl radical. *J Chem Phys* 122:104310.
18. Zhang B, Yan S, Liu K (2007) Unraveling multicomponent images by extended cross correlation analysis. *J Phys Chem A* 111:9263–9268.
19. Yoon S, Holiday RJ, Sibert EL, III, Crim FF (2003) The relative reactivity of CH_3D molecules with excited symmetric and antisymmetric stretching vibrations. *J Chem Phys* 119:9568–9575.
20. Duncan WT, Truong TN (1995) Thermal and vibrational-state selected rates of the $CH_4 + Cl \rightarrow HCl + CH_3$ reaction. *J Chem Phys* 103:9642–9652.
21. Corchado JC, Truhlar DG, Espinosa-Garcia J (2000) Potential energy surface, thermal, and state-selected rate coefficients, and kinetic isotope effects for $Cl + CH_4 \rightarrow HCl + CH_3$. *J Chem Phys* 112:9375–9389.
22. Rangel C, Navarrete M, Corchado JC, Espinosa-Garcia J (2006) Potential energy surface, kinetics, and dynamics study of the $Cl + CH_4 \rightarrow HCl + CH_3$ reaction. *J Chem Phys* 124:124306.
23. Wang X, Ben-Nun M, Levine RD (1995) Peripheral dynamics of the $Cl + CH_4 \rightarrow HCl + CH_3$ reaction. A classical trajectory computation. *Chem Phys* 197:1–17.
24. Zhou J, Zhang B, Lin JJ, Liu K (2005) Imaging the isotope effects in the ground state reaction of $Cl + CH_4$ and CD_4. *Mol Phys* 103:1757–1763.
25. Zhang B, Liu K (2005) Imaging a reactive resonance in the $Cl + CH_4$ reaction. *J Chem Phys* 122:101102.
26. Miller WH, Handy NC, Adams JE (1980) Reaction path Hamiltonian for polyatomic molecules. *J Chem Phys* 72:99–112.
27. Wardlaw DM, Marcus RA (1984) RRKM reaction rate theory for transition states of any looseness. *Chem Phys Lett* 110:230–234.
28. Zhou J, Lin JJ, Zhang B, Liu K (2004) On the $Cl^*(^2P_{1/2})$ reactivity and the effect of bend excitation in the $Cl + CH_4/CD_4$ reactions. *J Phys Chem A* 108:7832–7836.
29. Skodje RT, Skouteris D, Manolopoulos DE, Lee SH, Dong F, Liu K (2000) Observation of a transition state resonance in the integral cross section of the F + HD reaction. *J Chem Phys* 112:4536–4552.
30. Skodje RT, *et al.* (2000) Resonance-mediated chemical reaction: $F + HD \rightarrow HF + D$. *Phys Rev Lett* 85:1206–1209.
31. Liu K, Skodje RT, Manolopoulos DE (2002) Resonance in bimolecular reactions. *PhysChemComm* 5:27–33.
32. Lee SH, Dong F, Liu K (2002) Reaction dynamics of $F + HD \rightarrow HF + D$ at low energies: Resonant tunnelling mechanism. *J Chem Phys* 116:7839–7848.
33. Lee SH, Dong F, Liu K (2006) A crossed-beam study of the $F + HD \rightarrow HF + D$ reaction: The resonance-mediated channel. *J Chem Phys* 125:133106.
34. Bechtel HA, Kim ZH, Camden J-P, Zare RN (2004) Bond and mode selectivity in the reaction of atomic chlorine with vibrationally excited CH_2D_2. *J Chem Phys* 120:791–799.
35. Yoon S, Holiday RJ, Crim FF (2005) Vibrationally controlled chemistry: Mode- and bond-selected reaction of CH_3D with Cl. *J Phys Chem B* 109:8388–8392.
36. Zare RN (1998) Laser control of chemical reactions. *Science* 279:1875–1879.
37. Crim FF (1999) Vibrational state control of bimolecular reactions: Discovering and directing the chemistry. *Acc Chem Res* 32:877–884.
38. Atkins P, de Paula J (2002) *Atkins' Physical Chemistry* (Oxford Univ Press, Oxford), pp 968–969.

J. Phys. B: At. Mol. Opt. Phys. **41** (2008) 225001 (7pp) doi:10.1088/0953-4075/41/22/225001

Anisotropies of photoelectron angular distribution in the vicinity of autoionization resonances

Sandeep Tauro and Kopin Liu

Institute of Atomic and Molecular Sciences (IAMS), Academia Sinica, PO Box 23-166, Taipei 10617, Taiwan

E-mail: kliu@po.iams.sinica.edu.tw

Received 19 May 2008, in final form 19 August 2008
Published 10 November 2008
Online at stacks.iop.org/JPhysB/41/225001

Abstract

Using a photoelectron imaging technique, remarkable variations of photoelectron angular distributions are demonstrated in the region of autoionization resonance states of a two-photon excited I-atom. It is shown that the observed energy evolution of angular variation exhibits Fano-like behaviour and can be parametrized, for an isolated autoionization state, using the theoretically proposed scaling relationship for the width and the energy shift with respect to the absorption spectrum of the autoionizing state. In the case of overlapping resonances, however, it is found that the scaling relationship fails to account for the energy dependences of the β_4 parameters, though it remains valid for the β_2 spectra. Possible reasons are discussed.

1. Introduction

Asymmetric lineshape is ubiquitous in many atomic and molecular spectra [1, 2], as well as in condensed matter physics [3–7]. The universal character of this profile [8] is recognized as the manifestation of a quantum interference phenomenon, as first pointed out by U Fano in interpreting the autoionization spectra of rare gases [9]. Here, the process arises from the excitation to a discrete resonance state embedded in the ionization continuum. Thus, two competing optical pathways are possible: one path links the ground state to an excited discrete state, and the other connects the ground state with a continuum of energy states. The interference of two alternative pathways gives rise to typically an asymmetric profile of absorption cross sections as a function of energies, which can be expressed as the Fano formula [10, 11]:

$$\sigma = \sigma_b + \sigma_a(q+\varepsilon)^2/(1+\varepsilon^2). \quad (1)$$

Here σ_b is the excitation cross section for transitions into continuum that do not interact with the superexcited Rydberg state (i.e. the background absorption far away from resonance), σ_a is that for transitions into the continuum coupled to the Rydberg state and $\varepsilon = (E - E_r)/(\Gamma/2)$ is the reduced energy with E_r and Γ being the peak position and the width of the resonance, respectively. The dimensionless profile index or Fano parameter q measures quantitatively the degree of asymmetry of the resonance profile from the interference of the two alternative excitation pathways between resonant excitation and direct photoionization.

To gain a clear physical insight into the Fano formula (1), figure 1 summarizes the basic idea and the effects of the q value on the spectral profile. Depicted in figure 1(a) are the excitation mechanisms and the interference pathways, where C_1 and C_2 are the two alternative excitation amplitudes and C_{12} denotes the coupling amplitude between the discrete and continuum. In this scheme, the Fano parameter q corresponds to C_1^2/C_2C_{12}, thus, measures the strength of the coupling to the continuum. The decisive role of the q parameter in dictating the lineshape is illustrated for $q < 0$ in figure 1(b), where the relationship between the q value and the characteristic features (the extremes) of the spectral profile is explicitly shown. Also depicted in figure 1(b) are the cases for a positive q and the two limiting values, 0 and ∞. As can be seen, the symmetric Lorentzian peak is recovered when $q \to \infty$, i.e. when the coupling between the discrete state and the continuum (C_{12}) is vanishingly weak. On the other hand, when this coupling is strong and the transition probability to the discrete state is weak, then $q \to 0$ and a symmetric 'window resonance' is observed.

While the Fano formula (1) is well known and has been widely used to fit and interpret the asymmetric spectral peak, it is less documented for the other experimental observables.

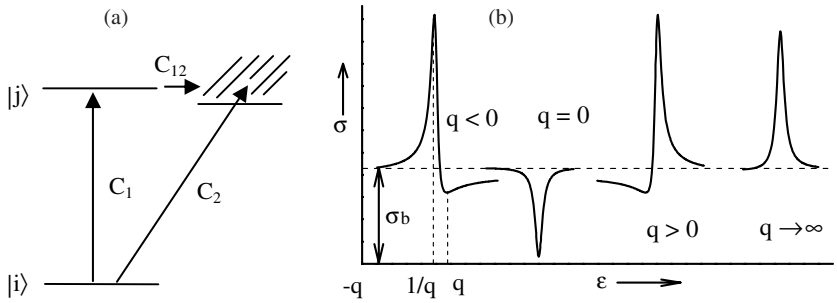

Figure 1. Schematic representation of the basic mechanism underlying the Fano lineshape (a), in which two indistinguishable pathways—a direct excitation C_2 and an indirect one through C_1 and the discrete–continuum coupling C_{12}—are possible to reach the same final continuum state. Four different profiles are shown in (b) to illustrate the effect of the profile index q on the spectral lineshape. Also exemplified in the case of $q < 0$ are the relationships between the characteristic features and the q value.

Since the absorption cross section (or the spectral profile) and the vector-correlation parameters are merely two sides of the same coin—both manifest the behaviour of ionization amplitudes—one may ask: When an autoionization peak shows pronounced asymmetric absorption profile and how does the other concomitant observable such as photoelectron angular distribution or the product ion polarization behaves across the autoionizing resonance peak? A recent work by Grum-Grzhimailo *et al* [12] addressed exactly such a question. They showed theoretically that in the region of an isolated autoionizing resonance state, the vector correlation parameters also exhibit the Fano-like behaviour, and the width and the peak position of the vector correlation observables possess universal scaling relationships to those encountered in the usual photoabsorption cross section. These predictions were validated by the concurrent experimental measurements of the alignment and orientation of the final photoion in the region of the Xe $4d_{5/2}^{-1}6p(J = 1)$ autoionizing resonance [12].

Recently, this laboratory reported a photoionization dynamics study of iodine atom using the photoelectron imaging technique [13]. Numerous autoionizing resonances were identified and a variety of photoelectron angular distributions were observed. During the course of that investigation, we noticed that the observed angular distribution appeared sensitively dependent on the exact photon energy, i.e. within 1 cm^{-1} of dye laser output. An in-depth investigation was then undertaken, which revealed peculiar yet systematic trends of photoelectron angular distributions across autoionizing peaks. In an effort of trying to understand those intriguing results, we came across the above paper by Grum-Grzhimailo *et al.* As reported here, their theoretical framework provides an insightful means to elucidate the underlying physics of our observations.

2. Experiment

As the experimental details have been presented previously [13, 14], only a brief description will be given here. A cold molecular beam was generated by expanding a gas mixture of ∼9.5% CH_3I in He at a total pressure of 30 psi via a fast opening Even–Lavie pulsed valve. The molecular beam, which was skimmed and collimated to ∼1 mm diameter along the ion time-of-flight axis, was intersected at right angle by a frequency-doubled laser beam. The laser was vertically polarized (i.e. parallel to the detector face) and focused by an $f = 50$ cm spherical lens to the centre between the repeller and extractor electrodes. In this one-colour experiment, the laser photolyzed CH_3I and ionized either the parent molecule [14] or the neutral photofragments—mainly the I-atom [13]. Electrons produced in the interaction region were probed by the velocity-map imaging technique [15, 16]. The non-uniformity of the detection sensitivity of the imaging system was corrected, following the procedure detailed previously [13]. The anisotropy coefficients, β_2 and β_4, of the photoelectron angular distribution were derived from fitting the Abel-inverted images [17].

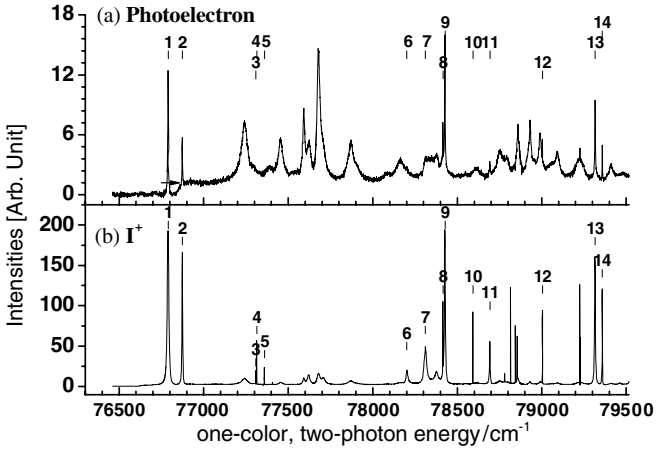

Figure 2. The photoelectron spectrum (a) and the photoionization spectrum of the fragment I-atom (b) following the photodissociation of CH_3I. The numbers label the spectral peaks of the iodine atom (see [13]).

3. Results and analysis

3.1. Autoionization spectral profile

To set the stage, figure 2 displays two photoionization spectra by (a) monitoring the photoelectron and (b) detecting the iodine cation as in previous reports [13, 14]. The peak numbers label (some of) the atomic iodine transitions over this energy range. As discussed previously [13], those peaks arise from

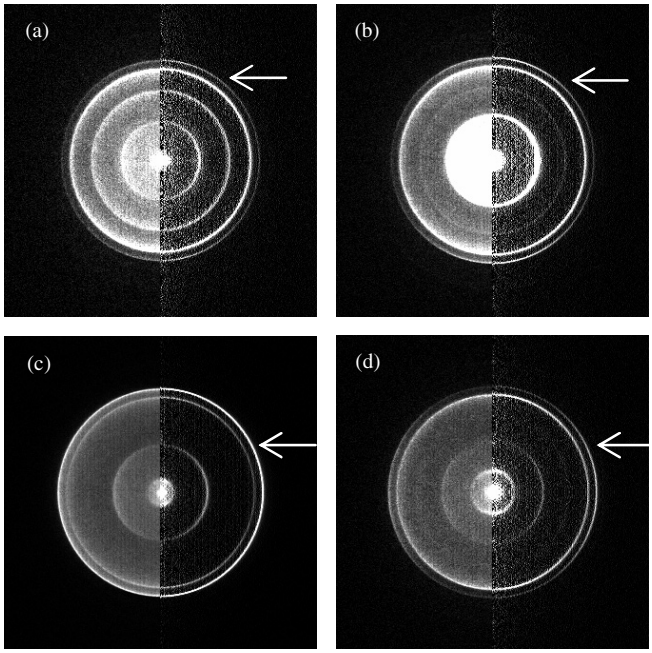

Figure 3. Four representative photoelectron images at two-photon energies near peak 6, with (a)–(d) marked in figure 4. In each panel, the left half displays the raw image and the right half shows the Abel-inverted one. The laser polarization axis is vertical in the plane. The arrows point to the ring feature arising from the autoionization process of the I-atom. The other ring structures can be assigned to the vibronic autoionization of the CH_3I molecule [14].

two types of photoionization processes: the (2+1) resonance-enhanced multiphoton ionization (REMPI) process of the ground state $I(^2P_{3/2})$ atom and the two-photon transitions originating from the spin–orbit excited state $I(^2P_{1/2})$ and terminating in superexcited Rydberg (or autoionization) states I^{**} that converge to the $I^+(^3P_1)$ ionization threshold. The latter peaks are of concern in this study, namely, the autoionization process of

$$I(^2P_{1/2}) + 2h\nu \rightarrow [I^{**}] \rightarrow I^+(^3P_2) + e^-. \quad (2)$$

Figure 3 shows four photoelectron images acquired at different laser wavelengths in the vicinity of peak 6. In each panel, the left half displays the raw image and the right half shows the Abel-inverted one [13, 15]. On energetic grounds, the multi-ring features can readily be assigned to the photoionization of either the parent molecule CH_3I [14] or the I-fragment (indicated by the arrow) [13], from which the fraction of the latter intensity to the total intensity can then be determined. To recover the photoionization spectrum of our interest, process (2), from the total photoelectron spectrum shown in figure 2(a), numerous photoelectron images across a given spectral peak were taken and the dependence of the intensity fraction on photon energy was then determined. Figure 4 shows such results for peak 6. Displayed in the upper panel are the energy dependences of the total electron intensity and the fraction coming from process (2); the resultant autoionization spectral profile is presented in the lower panel. Also shown in the lower panel is the photoionization spectrum of the same peak by monitoring the cation I^+ (figure 2(b)). Clearly, the I^+-spectrum is considerably narrower, suggesting that other processes, such as multiphoton ionization of CH_3I followed by dissociation, are taking place [13] and contribute to the observed I^+ signals, thus distorting the spectral profile. Note by passing that figure 3 gives a clear demonstration of the power of the ion (or electron) velocity map imaging technique in unravelling the desired ionization process from other concomitantly occurring processes.

3.2. *Isolated resonance*

The angular distributions from the autoionization process (2), indicated by arrows in figure 3, exhibit a dramatic dependence on photon energies. For example, it changes from predominantly positive β values in (a) and (b) to a nearly isotropic one in (c), and further to a clearly negative β parameter in (d). Since a two-photon transition is invoked in process (2), the angular distribution was analysed by the expression [18–20]

$$I(\theta) \propto \beta_2 P_2(\cos\theta) + \beta_4 P_4(\cos\theta). \quad (3)$$

Here $P_2(\cos\theta)$ and $P_4(\cos\theta)$ are the Legendre polynomials of degrees 2 and 4, respectively, β_2 and β_4 are the corresponding anisotropy coefficients and θ is the angle between the directions of the laser polarization and the ejected electron. The best-fitted distributions (the solid lines) along with the experimental data for the four images in figure 3 are displayed in the polar representation in the upper panel of figure 5(a). The lower portion of figure 5 summarizes the best-fitted β_2 and β_4 coefficients over the spectral profile of peak 6. It is quite remarkable that the photoelectron angular distributions, or the β_2 and β_4 coefficients, exhibit such dramatic variations across an autoionization resonance.

Similar measurements and analysis were performed for peak 11, and the final results are presented in figure 5(b). Peaks 6 and 11 have been assigned [13] to the transitions from $^2P_{1/2}$ to $(^3P_1)8p[2]_{5/2}$ and to $(^3P_1)8p[2]_{3/2}$, respectively. (The notation of the superexcited Rydberg state follows the $J_c l$ coupling scheme [21], in which the total angular momentum J_c of the I^+ ion core is coupled to the orbital angular momentum l of the Rydberg electron to give the resultant K. The spin, s, of the Rydberg electron is then coupled to K to give the total angular momentum J. The state is thus labelled as $(^3P_{J_c})nl[K]_J$.) Therefore, the observed autoionization process (2) corresponds to ejecting the 8p Rydberg electron to form the final ion state $I^+(^3P_2)$. Since the ion-core state changes from $^3P_1$ to $^3P_2$, this autoionization process must invoke the spin–orbit couplings of the $^3P_1$-core Rydberg states to the $^3P_2$ ion-continuum. Physically, it can arise from either the spin-flip in the core to release the Rydberg electron or the exchange interactions between the Rydberg and core electrons [22, 23].

Assuming a Coulomb repulsive form for the autoionization interaction matrix and approximating it as a two-electron problem, a propensity rule of $\Delta l = 0, \pm 2$ for autoionizing electrons has previously been derived [13]. For the p-like Rydberg states, such as the present peaks 6 and 11, the dominant outgoing electron waves will be of the p and f types. Hence, the observed variations of the photoelectron angular distributions across the autoionization states seen in figure 5 arise from the interferences of the two outgoing waves

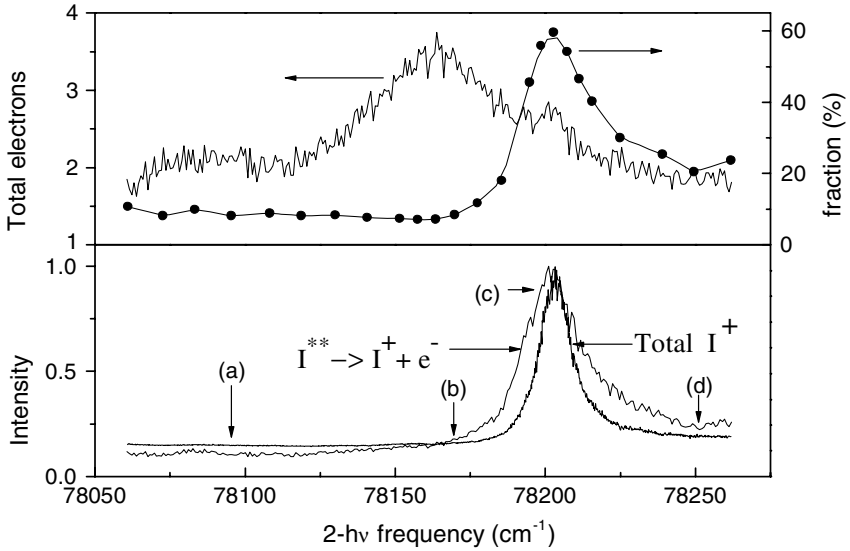

Figure 4. The upper panel presents the photoelectron yield spectrum of peak 6 and the fractional branching (·) of the total electrons that is from autoionizing the I-atom. The lower panel shows the resultant photoelectron yield spectrum for process (2), along with the photoionization spectrum of the I-atom by monitoring I^+. For comparison, both spectra are normalized to the same peak heights.

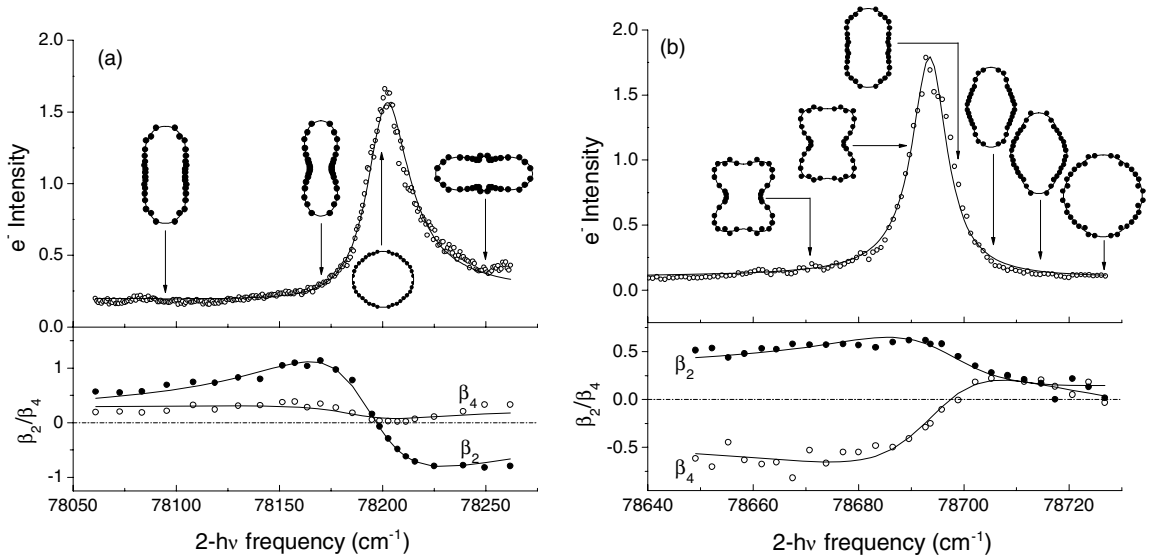

Figure 5. Summary of the autoionizing lineshape and the anisotropy coefficients of photoelectron angular distribution for peak 6 in (a) and peak 11 in (b). The points are the experimental data and the lines are the fits (see the text for details). Also exemplified in the upper panels are a few photoelectron angular distributions in the polar representation at different energies marked by arrows.

whose magnitudes and phases are continuously changing as the photon energy changes. Note that even at energies relatively far away from the resonance peak, the two-photon ejected 'background' f-wave could conceivably invoke a shape resonance trapped by the $l = 3$ centrifugal barrier—in contrast to the Feshbach type associated with an autoionizing resonance—so that the rapid variation of the phase shift of the direct ionization amplitude might need to be considered. It is also worth noting that while the states for peaks 6 and 11 invoke the same Rydberg orbital and the same K, the degrees of asymmetry of their lineshapes are clearly different, so as the patterns of photoelectron angular distributions. Inspection of the displayed photoelectron angular distributions suggests more f-wave characters for peak 11 than peak 6. Further theoretical work will be needed to understand this intriguing J-dependence of the discrete–continuum couplings.

The observed asymmetric lineshapes (the upper panels, figure 5) can be parametrized using the Fano profile expression (equation (1)). The resultant fits are shown as the solid lines in figure 5, and the parameters summarized in table 1. Since this is a multi-variable fit to equation (1), the choices of initial parameters were guided by the extremes, such as the magnitude of the absorption cross section far from the peak for σ_b as well the peak position/width and the degree of asymmetry

Table 1. Fano parameters in fitting the two-photon absorption cross section, equation (1) or (6), and the anisotropy coefficients of the photoelectron angular distribution, equation (4) or (7). See the text for details. Note that the ionization potential (IP) of the iodine atom is 84 295.1 cm^{-1} [21] and that of the spin–orbit excited $I(^2P_{1/2})$ is 7603.2 cm^{-1} above the ground state $I(^2P_{3/2})$; thus, the listed autoionization states range from about 97 cm^{-1} to 2666 cm^{-1} above the IP for peaks 1 and 14, respectively.

Parameters		Peak 6	Peak 11	Peak 1/2	Peak 13/14
	E_r (cm^{-1})	85 803.98	86 296.85	84 392.05/84 476.65	86 918.55/86 961.45
	Γ (cm^{-1})	24.7	8.1	4.95/4.4	5.45/2.5
σ	σ_b	0.19	0.12	0.044	0.14
	σ_a	0.019	0.0011	0.0036/0.0023	0.0051/0.0041
	q	8.34	−39.7	−54/43	−36/29.2
	Δ (cm^{-1})	−9.36	+1.46	+10.1/−4.7	+3.44/−1.03
	Γ (cm^{-1})	63.7	31.5	70.83/41.3	36.51/12.4
β_2	σ_b'	0.67	0.58	0.49	0.41
	σ_a'	−1.11	−0.29	0.44/−0.41	0.32/−0.39
	q'	0.84	0.62	−0.5/0.28	−0.43/0.21
	Δ (cm^{-1})	−9.36	+1.46	−3.8/−73.5	−2.4/−33.1
	Γ (cm^{-1})	63.7	31.5	15/80	15/50
β_4	σ_b''	0.11	−0.65	−0.2	−0.41
	σ_a''	0.16	0.31	0.27/−0.001	0.21/−0.0025
	q''	−0.46	1.31	1.11/11.6	1.34/17.7

for q, as illustrated in figure 1(b). The listed parameters were then yielded after several iterations for the global fit. The uncertainties for E_r and Γ are within 1 cm^{-1}, whereas the three parameters σ_a, σ_b and q are highly correlated with the estimated uncertainty of ± 2 for the q value. It is worth noting that from the fitted widths Γ, the effective autoionization lifetimes of the $(^3P_1)8p[2]_{5/2}$ (peak 6) and $(^3P_1)8p[2]_{3/2}$ (peak 11) Rydberg states can be estimated to be 0.22 ps and 0.65 ps, respectively. Compared to peak 6, the profile of peak 11 appears more symmetric, which yields a larger value of $|q|$. Since $q = C_1^2/C_2C_{12}$ and from table 1, an estimated $\sigma_a(=C_1^2)$ for peak 11 is an order of magnitude smaller than that for peak 6; a larger $|q|$ will then imply a significantly smaller value of C_2 and/or C_{12}. However, from table 1 the estimated $\sigma_b(=C_2^2)$ for the two peaks are comparable; thus, the Rydberg–continuum coupling (C_{12}) for peak 11 must be weaker than that for peak 6, in consistence with the above longer lifetime.

In order to analyse in detail the measured photoelectron angular distribution, we followed the theoretical prediction of Grum-Grzhimailo *et al* [12] by expressing the anisotropy coefficients in terms of a Fano-like form:

$$\beta_i = \sigma_b^{\beta_i} + \sigma_a^{\beta_i}(q^{\beta_i} + \tilde{\varepsilon})^2/(1 + \tilde{\varepsilon}^2). \tag{4}$$

In equation (4) the parameters $\sigma_b^{\beta_i}$, $\sigma_a^{\beta_i}$ and q^{β_i} are specific quantities for each individual observable β_i. However, the scaled energy $\tilde{\varepsilon} = (E - \tilde{E}_r)/(\tilde{\Gamma}/2)$ in equation (4) is fixed by a scaled width $\tilde{\Gamma} = x\Gamma$, and the shifted resonance energy $\tilde{E}_r = E_r + \Delta$ from fitting the spectral profile (equation (1)) with $x = [\sigma_b(\sigma_0 + \sigma_a q^2)]^{1/2}/\sigma_0$, $\Delta = -(q\Gamma\sigma_a)/2\sigma_0$ and $\sigma_0 = \sigma_a + \sigma_b$ [12]. The resultant fits to the energy dependences of the anisotropy coefficients for both peaks 6 and 11 are displayed as the solid lines in the respective lower portions of figure 5, and the parameters are also listed in table 1. As can be seen, the energy dependences of both β_2 and β_4 are reasonably reproduced, despite vastly different behaviours. More remarkable is the fact that the two parameters $\tilde{\Gamma}$ and $\tilde{E}_r$ used in fitting both β_2 and β_4 spectra follow exactly the universal scaling relationships given above, in strong support of the theoretical prediction.

An alternative approach to account for the variation in β over an autoionizing resonance is the so-called KS formula [24, 25], which is derived for the one-photon ionization processes. In that framework

$$\beta = -2(X\varepsilon^2 + Y\varepsilon + Z)/(A\varepsilon^2 + B\varepsilon + C), \tag{5}$$

and the coefficients A, B and C are related to the Fano parametrization for the photoionization cross section, equation (1), as $A = \sigma_a + \sigma_b$, $B = 2q\sigma_a$ and $C = \sigma_a q^2 + \sigma_b$. The coefficients X, Y and Z are treated as free parameters in the fit to the data. (Note that either equation (4) or (5) involves three fitting parameters.) While we found that the KS formula can also be adopted in fitting the β_2 spectra for peaks 6 and 11, its theoretical validity to fit the β_4 spectrum is yet to be established. Moreover, the use of equation (5) becomes ambiguous in the case of overlapping resonances (*vide infra*). We therefore did not pursue further along that line.

3.3. Overlapping resonances

Figure 6 (the upper panels) presents two pairs of autoionizing resonances, peaks 1 and 2 in (a) and peaks 13 and 14 in (b). The two peaks in each pair appear well separated, yet not far enough to allow a separated fitting to each individual peak according to equation (1). To *simultaneously* fit the pair of overlapping resonances, we tentatively used a Fano-like form:

$$\sigma = \sigma_b + \sigma_{a_1}(q_1 + \varepsilon_1)^2/(1 + \varepsilon_1^2) + \sigma_{a_2}(q_2 + \varepsilon_2)^2/(1 + \varepsilon_2^2). \tag{6}$$

In other words, we assumed that the direct couplings between the two resonance states are negligibly small, yet both resonances are coupled to a common continuum. The results are shown as solid lines in the upper portions of figure 6, and the fitting parameters are listed in table 1. From the fitted widths Γ, the effective lifetimes of those autoionization states range from about 2.1 ps for peak 14 to 0.97 ps for peak 13,

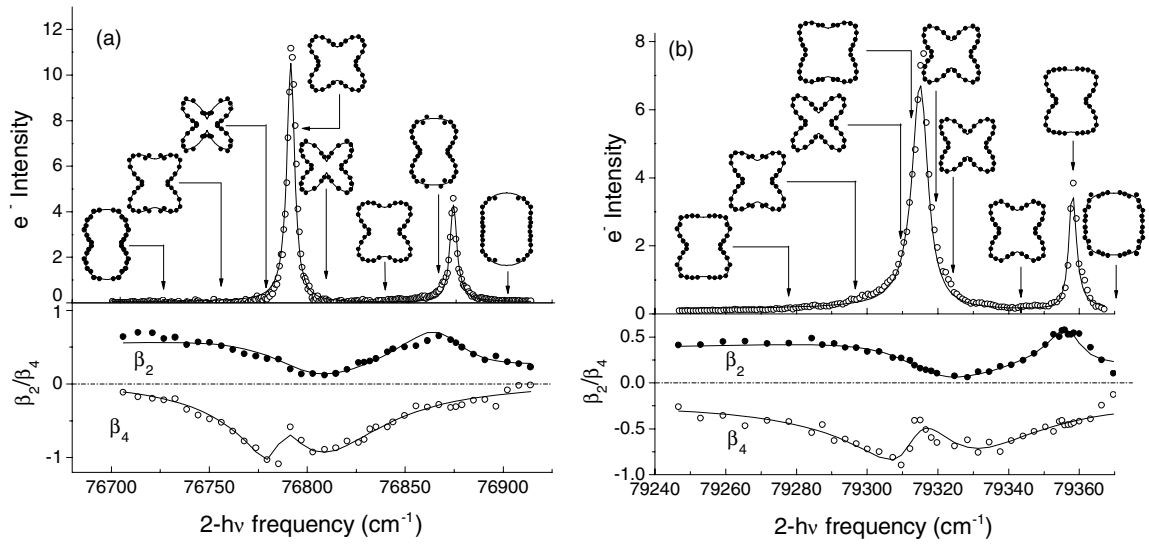

Figure 6. Same as figure 5, but for two pairs of overlapping resonance states: (a) for the pair of peaks 1 and 2, and (b) for peaks 13 and 14. Note that the width and shift in fitting the β_2 spectra follow the scaling relationships, but they are treated as free parameters for the fitted β_4 spectra.

i.e. somewhat longer than the above isolated resonances. More rigorous treatment will have to be rendered to theoretical works on overlapping resonances [26, 27].

The energy dependences of the corresponding anisotropy coefficients are shown in the lower panels. An analogous form is assumed in fitting the β spectra, i.e.

$$\beta_i = \sigma_b^{\beta_i} + \sigma_{a_1}^{\beta_i}\left(q_1^{\beta_i} + \tilde{\varepsilon}_1\right)^2 \Big/ \left(1 + \tilde{\varepsilon}_1^2\right) + \sigma_{a_2}^{\beta_i}\left(q_2^{\beta_i} + \tilde{\varepsilon}_2\right)^2 \Big/ \left(1 + \tilde{\varepsilon}_2^2\right). \tag{7}$$

Note that the universal scaling relationships proposed by Grum-Grzhimailo are formulated for an *isolated* resonance; it is not clear a prior if they will also hold for overlapping resonances. Nevertheless, using the universal scaling relationships, we found that equation (7) can reproduce the energy dependences of the β_2 parameters for both pairs (shown as the solid lines in the lower portions of figure 6), but it failed to account for the β_4 spectra—in particular for the peculiar, central peaking behaviour around the resonance energy of peaks 1 and 13, respectively. However, if the shifts and the widths for β_4 are treated as free parameters, the energy dependences of β_4 can be reasonably reproduced by equation (7), as shown by the solid lines in figure 6.

Two plausible reasons can be offered for the failure of the universal scaling relationship in fitting the β_4 parameters. Firstly, the expression of equation (6) or equation (7) assumes a case of two non-interacting resonance states coupled to one continuum. Hence, its form may not be applicable if the coupling between the two overlapping resonances cannot be neglected. Secondly, the autoionization states for peaks 1 and 2 are $(^3P_1)4f[2]_{3/2,5/2}$ and $(^3P_1)4f[3]_{5/2}$, respectively [13, 21]. In other words, accounting for the two fine-structure states hidden underneath peak 1, three resonance states are actually involved—rather than two resonances as implicated in equations (6) and (7). Two of them are, however, not resolvable in the photoelectron spectra (i.e. shown as peak 1) nor can they manifest themselves as any noticeable feature in the energy dependences of the β_2 parameters, which suggests that the direct coupling between the two heavily overlapped resonances may need to be considered, rendering the mere addition of a third resonance term in equations (6) and (7) inadequate. Further theoretical works will be required. Nevertheless, the observation of an intriguing local structure near peak 1 in the energy dependence of β_4 seems to suggest this as a more likely explanation. Based on the previously derived propensity rule $\Delta l = 0, \pm 2$ for autoionization [13], the f-like Rydberg state will preferentially eject p-, f- and h-waves. Thus, three outgoing waves are involved in the vicinity of each autoionization resonance state, and nine waves in total need to be considered over the energy range of figure 6. More perplexing interference patterns are anticipated. Inspection of the exemplified angular distributions in the upper panel of figure 6(a) indicates that it is indeed the case. Similarly, the autoionization states for peaks 13 and 14 are $(^3P_1)5f[2]_{3/2,5/2}$ and $(^3P_1)5f[3]_{5/2}$, i.e. the same respective Rydberg series as peaks 1 and 2 [13]. It is therefore not too surprising to note that the general patterns of β_2 and β_4 spectra, or the overall shapes of the positive β_2 and negative β_4 values, are remarkably similar for the pair of peaks 1 and 2 and peaks 13 and 14.

4. Summary

An in-depth study of autoionizing dynamics of the iodine atom by two-photon excitation was carried out using the photoelectron imaging technique. Particular emphasis is placed on the energy dependences of the ejected photoelectron angular distributions. A dramatic variation was found in the vicinity of autoionization resonance states. Exploiting the scaling relationship predicted theoretically, the energy evolutions of the observed anisotropy coefficients can be accounted for in the case of isolated resonances. However, in the case of overlapping resonances, while the scaling relationship remains held for the β_2 parameters, it fails to

reproduce the β_4 behaviours. Possible explanations are suggested, and further theoretical investigations are warranted.

Acknowledgments

We gratefully acknowledge the contributions of Dr C Hu to the initial phase of this project and of Dr S Pei for his helps in acquiring the data. This work was supported in parts by National Science Council of Taiwan (NSC 96-2628-M-001-016-NY3), Academia Sinica (AS Investigator Award 2371), and the US Air Force Office of Scientific Research (AOARD-07-4005).

References

[1] Fano U and Cooper J W 1968 *Rev. Mod. Phys.* **40** 441
[2] Connerade J P and Lane A M 1988 *Rep. Prog. Phys.* **51** 1439
[3] Neuhauser D, Park T J and Zink J I 2000 *Phys. Rev. Lett.* **85** 5304
[4] Faist J, Capasso F, Sirtori C, West K W and Pfeiffer L N 1997 *Nature* **390** 589
[5] Song J F, Ochiai Y and Bird J P 2003 *Appl. Phys. Lett.* **82** 4561
[6] Hase M, Demsar J and Kitajima M 2006 *Phys. Rev.* B **74** 212301
[7] Bar-Ad S, Kner P, Marquezini M V, Mukamel S and Chemla D S 1997 *Phys. Rev. Lett.* **78** 1363
[8] Beutler H 1935 *Z. Phys.* **93** 177
[9] Fano U 1935 *Nuovo Cimento* **12** 156
[10] Fano U 1961 *Phys. Rev.* **124** 1866
[11] Fano U and Cooper J W 1965 *Phys. Rev.* **137** A1364
[12] Grum-Grzhimailo A N, Fritzsche S, O'Keeffe P and Meyer M 2005 *J. Phys. B: At. Mol. Opt. Phys.* **38** 2545
[13] Hu C, Pei S, Chen Y-L and Liu K 2007 *J. Phys. Chem.* A **111** 6813
[14] Hu C, Pei S, Chang C and Liu K 2008 *Mol. Phys.* **106** 405
[15] Eppink A T J B and Parker D H 1997 *Rev. Sci. Instrum.* **68** 3477
[16] Lin J J, Zhou J, Shiu W and Liu K 2003 *Rev. Sci. Instrum.* **74** 2495
[17] Dribinski V, Ossadtchi A, Mandelshtam V A and Reisler H 2002 *Rev. Sci. Instrum.* **73** 2634
[18] Lambropoulos P 1976 *Adv. At. Mol. Phys.* **12** 87
[19] Dixit S N and Mckoy V C 1985 *J. Chem. Phys.* **82** 3546
[20] Suzuki T and Whitaker B J 2001 *Int. Rev. Phys. Chem.* **20** 213
[21] Minnhagen L 1962 *Ark. Fys.* **21** 415
[22] Berkowitz J 1988 *Adv. Chem. Phys.* **72** 1
[23] Berkowitz J 1979 *Photoabsorption, Photoionization and Photoelectron Spectroscopy* (New York: Academic)
[24] Kabachnik N M and Sazhina I P 1976 *J. Phys. B: At. Mol. Phys.* **9** 1681
[25] Taylor K T 1977 *J. Phys. B: At. Mol. Phys.* **10** L699
[26] Mies F H 1968 *Phys. Rev.* **175** 164
[27] Chang T N and Zhu L 1993 *Phys. Rev.* A **48** R1725

PCCP

Physical Chemistry Chemical Physics

www.rsc.org/pccp

Volume 10 | Number 30 | 14 August 2008 | Pages 4349–4504

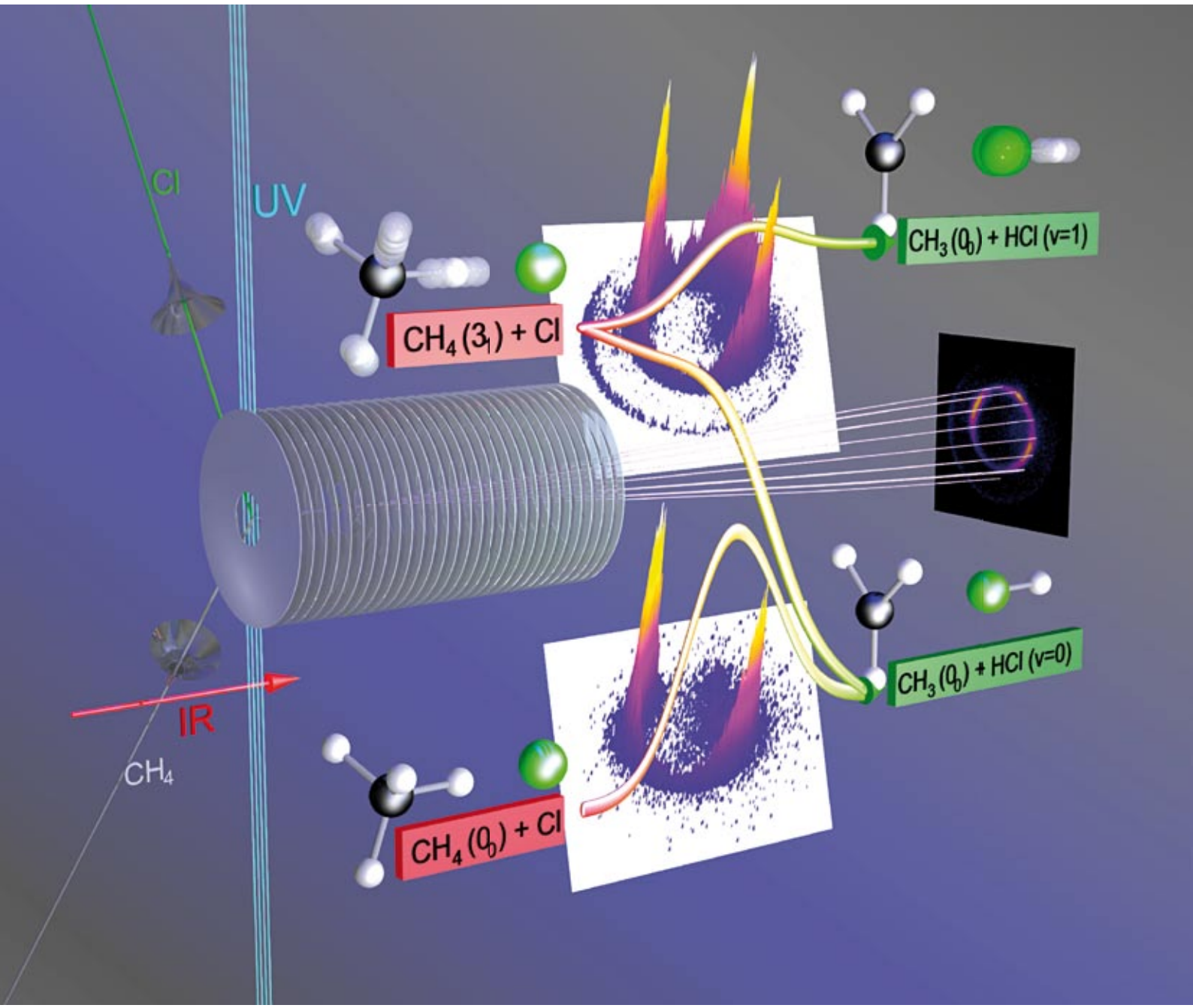

ISSN 1463-9076

COVER ARTICLE
Kawamata *et al.*
Unravelling the reactivity of antisymmetric stretch-excited CH_4 with Cl by product pair-correlation measurements

HOT ARTICLE
Wang *et al.*
On the lifetimes and physical nature of incompletely relaxed electrons in liquid water

Unravelling the reactivity of antisymmetric stretch-excited CH_4 with Cl by-product pair-correlation measurements

Hiroshi Kawamata, Sandeep Tauro and Kopin Liu

Received 2nd June 2008, Accepted 10th June 2008
First published as an Advance Article on the web 24th June 2008
DOI: 10.1039/b809209e

The vibrational branching ratio $[CH_3(v = 0) + HCl(v' = 1)]/[CH_3(v = 0) + HCl(v' = 0)]$ of two correlated product pairs from the title reaction shows a dramatic E_c-dependence, in sharp contrast to the previously observed behavior in Cl + CHD_3-($v_1 = 1$), while the vibrational enhancement factors in reactivity of the two reactions are remarkably similar.

It has been well documented, both experimentally[1–11] and theoretically,[12–18] that excitation of different vibrational motions of a polyatomic reactant can exert profound effects on chemical reactivity. What emerged from those mode-selective studies is the intuitively appealing picture that, in a direct bimolecular reaction, the vibrational state containing large components of motion along a particular reaction coordinate preferentially drives the system over the transition state along that coordinate, leading to mode-dependent reactivity and product branching ratios. Among the systems that have been studied, the reaction of chlorine atom with methane and its isotopic variants stands as a benchmark.[5–16] In the context of mode-specific behaviors, the reaction with CH_4 is of interest in that CH_4 has two nearly degenerate stretching modes, the symmetric (v_1) and the antisymmetric (v_3), and it is not totally clear, *a priori*, which mode will be more effective in promoting the reaction rate. At the outset, we should point out that the vibrational eigenstates are named by their dominant zero-order state characters. The nominal v_1 and v_3 fundamental stretching modes of CH_4 contain small admixture of bending mode character ($\sim$4–8% of contributions) in higher order polyads.[19,20]

In a pioneering work,[5] Zare and coworkers examined the effect of antisymmetric stretch excitation of $CH_4(v_3 = 1)$ on the reaction cross section and scattering dynamics and obtained a vibrational enhancement of 30 ± 15 at a mean collision energy $E_c = 15.5$ kJ mol^{-1}, which was attributed to the opening of the cone of acceptance of the reaction upon vibrational excitation.[21] A very recent re-investigation refined the enhancement factor to 13.4 ± 2.4.[22] A later study from the same laboratory compared the dynamical effects of symmetric (v_1) and antisymmetric (v_3) stretch excitations of CH_4 in Cl + CH_4.[6] They found that both stretching excitations yield virtually identical product internal state and angular distributions. Based on these observations, they concluded that, whereas the initial preparation of CH_4 in different stretching modes might alter the total reactivity (*vide infra*), the dynamics leading to product formation follow a common pathway, which could be promoted by vibrational mixing during the collision event, scrambling the initial mode-selection.

In that study, the infrared (IR)-inactive $v_1 = 0 \rightarrow 1$ excitation of CH_4 was achieved by stimulated Raman pumping. Comparison of its reactivity enhancement to the v_3-excitation could not be made because the fraction of methane molecules being pumped was not quantified. The difficulty of comparing the relative reactivities of the two fundamental stretching modes was alleviated by Crim and coworkers in studying the two stretch-bend combination vibrations of CH_4, $v_1 + v_4$ and $v_3 + v_4$ (v_4 is the umbrella bending vibration), for which both modes can be activated by direct IR excitations.[7] They observed a noticeable difference in reactivities: $\sigma(v_1 + v_4) = 1.9 \times \sigma(v_3 + v_4) = 19 \times \sigma(v = 0)$, arguing different reaction paths for the two types of vibrational excitations. They further proposed a vibrationally adiabatic model to rationalize the differential reactivities of the two modes of excitation.[7,18] In this model, the approach of the Cl-atom causes the vibrational energy of the CH_4 symmetric and antisymmetric stretches to become localized in the proximal (reactive) and distal (unreactive) C–H bonds, respectively. Thanks to this collision-induced intramolecular vibration energy redistribution (IVR), the symmetric stretch has more energy along the reaction coordinate, leading to a higher reactivity than the antisymmetric stretch excitation. In other words, the reaction remains largely vibrationally adiabatic without significant state mixing of two *local* modes during reactive collisions. Since there may be a synergic effect when a combination mode is excited, the subtle differences between the above two viewpoints (*i.e.*, same reaction path or not and the nature of mode mixings) remain to be reconciled.

Another motivation for initiating the present study is from one of our earlier works on the ground-state reaction.[23] Examining the E_c-evolution of two product pair-correlated angular distributions over a wide energy range from about 8.4 kJ mol^{-1} to 84 kJ mol^{-1} revealed vastly distinct patterns. While the result for the $CH_3(v = 0) + HCl(v' = 0)$ pair shows a pronounced ridge-structure suggestive of peripheral dynamics for a reaction governed by large impact-parameter collisions,[24,25] that for the $CH_3(v = 0) + HCl(v' = 1)$ pair exhibits a pattern characteristic of resonance reaction mechanism.[26] Based on previous *ab initio* calculations,[12,13] the correlation between the reactant and product vibrational modes was then constructed.[11,23] A dynamic potential well correlating the reactant Cl + $CH_4(v_1 = 1)$ to the $CH_3(v = 0)$ + $HCl(v' = 1)$ product pair was found, in support of the proposed reactive resonance mechanism. The reaction of Cl + $CH_4(v = 0)$ is, however, largely vibrationally adiabatic even at $E_c \sim 84$ kJ mol^{-1}; namely, more than 98% of reactive

Institute of Atom and Molecular Sciences (IAMS), Academia Sinica, P. O. Box 23-166, Taipei, Taiwan 10617

fluxes proceed through the vibrational ground-state reaction path leading to the $CH_3(v = 0) + HCl(v' = 0)$ product pair.[23] Thus, merely 2% of reactive trajectories are mediated by reactive resonance. To shed more light on the proposed reactive resonance, it is then desirable to initiate the reaction with $CH_4(v_1 = 1)$ for better access of the dynamic well. However, an efficient Raman pumping for $v_1 = 1$ excitation is more demanding. If the aforementioned collision-induced IVR[7,18] or the mode-mixing mechanism[6] is at work, an investigation with direct IR-pumped $CH_4(v_3 = 1)$ could then be a viable alternative.

Reported here is the first product pair-correlation measurement of the $Cl + CH_4(v_3 = 1) \rightarrow CH_3(v = 0) + HCl(v' = 0,1)$ reaction. The ground-state reaction of $Cl + CH_4$ is endothermic by 5.1 kJ mol^{-1}, with a reaction barrier about 10.5 kJ mol^{-1},[25] whereas one quantum of excitation in the v_1 and v_3 modes provides CH_4 molecule with energy equivalent to 34.9 kJ mol^{-1} and 36.1 kJ mol^{-1}, respectively. To elucidate the mode-specific behavior of this reaction, comparisons were made to both the ground-state reaction[23] and the analogous reaction of Cl-atom with C–H stretch-excited $CHD_3(v_1 = 1)$.[11] The latter comparison serves as a conceptually interesting contrast in that the initially prepared $CH_4(v_3 = 1)$ is a delocalized normal-mode vibration, whereas for $CHD_3(v_1 = 1)$ the vibrational energy is directly deposited into the localized C–H bond that is to be broken. These close scrutinies reveal rather different behaviors, which in turn lead to a new perspective about the effects of the two different stretching modes.

The experimental details are the same as the previous study on $Cl + CHD_3(v_1 = 1)$,[11] only a brief description is given here. A discharge-generated, pulsed Cl-beam (5% Cl_2 in He at 6 atm total pressure) was double-skimmed before crossing with a CH_4 beam pulsed from another valve. A tunable IR optical parametric oscillator/amplifier (OPO/A), operated in near single-mode, prepared the CH_4 reactant prior to the collision center with one-quantum excitation of antisymmetric stretch *via* the $v_3 = 0 \rightarrow 1$, R(1) transition at 3038.50 cm^{-1}.[27] The absolute frequency of the OPO/A output was calibrated with the aid of a photoacoustic cell filled with ~70 torr CH_4. After the collision, the dominant $CH_3(v = 0)$ product was probed by a (2+1) resonance-enhanced multiphoton ionization (REMPI) process at 333.57 nm *via* the 0_0^0-band of the $\tilde{X}^2A_2'' \rightarrow 3p_z^2A_2''$ Rydberg transition,[28] and a time-sliced ion velocity imaging technique[29] mapped the state-correlation of coincidently formed HCl coproducts.[11,30,31] The initial collision energy E_c was controlled by varying the intersection angles of the two molecular beams. To interrogate the effects of reactant vibrational excitation, at each E_c the product images were acquired with IR laser on and off alternatively to minimize the long-term drifts and other possible systematic errors.

Fig. 1(a) and (b) exemplify two raw images, IR-on and IR-off, at $E_c = 24.3$ kJ mol^{-1}. The IR-off image is virtually identical to that acquired previously:[23,25] the sideway-dominant ringlike feature is the $CH_3(v = 0) + HCl(v' = 0)$ product pair with small contribution, along the outer rim, of the same pair from reaction with bend-excited CH_4. (Supersonic expansion yields a translationally and rotationally cold (~5–10 K) methane beam, but with thermally populated vibration manifolds.[10]) When the IR laser is turned on, two new features are vividly displayed. On energetic grounds, the outer ring is ascribed to the $Cl + CH_4(v_3 = 1) \rightarrow CH_3(v = 0) + HCl(v' = 0)$ reaction (denoted as the $(0_0, 0)^{\neq}$ product pair with the supercript $\neq$ indicating the stretch-excited reactant) and the intense, sharp forward peak in the inner ring is from the $CH_3(v = 0) + HCl(v' = 1)$ or the $(0_0, 1)^{\neq}$ pair, which is nearly degenerate to the $(0_0, 0)$ pair from the ground-state reaction (IR-off image).

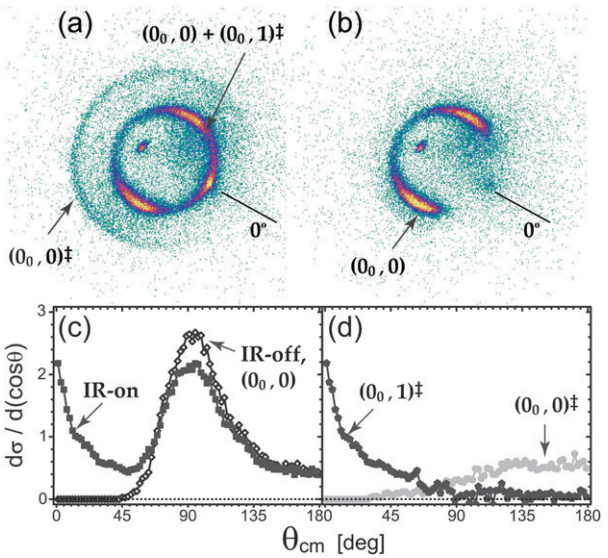

Fig. 1 Time-sliced raw images of the probed $CH_3(v = 0)$ products from the $Cl + CH_4$ reaction at $E_c = 24.3$ kJ mol^{-1} for IR-on (a) and IR-off (b). The 0°-angle is the initial direction of the CH_4 beam in the center-of-mass (cm) frame. The ringlike features of the product images are assigned as indicated. Some backgrounds such as the bright spot in the backward direction can readily be identified and were discounted in the data analysis. (c) The angular distributions of the inner ring structures from IR-on (a) and IR-off (b), respectively. (d) The derived angular distributions of the $(0_0, 1)^{\neq}$ and $(0_0, 0)^{\neq}$ product pairs from the $Cl + CH_4(\nu_3 = 1)$ reaction.

To disentangle the overlapped contributions to the inner ring of the IR-on image, we followed the approach recently developed in the studies of the $Cl + CHD_3(v_1 = 1)$ reaction.[11,32] Using the threshold method,[32] we obtained about 19% of CH_4 reactants being stretch-excited. By scaling down the IR-off angular distribution by 0.19 and subtracting it from the IR-on data (Fig. 1(c)), the genuine distribution for $(0_0, 1)^{\neq}$ was then recovered from the overlapped inner ring. The resultant pair-correlated angular distributions are presented in Fig. 1(d), which show vastly different appearances from the $(0_0, 0)^{\neq}$ pair, strongly suggesting different reaction pathways. A broad back/sideways angular distribution signifies a direct rebound mechanism[25] in forming the $(0_0, 0)^{\neq}$ product pair at this collisional energy, whereas a sharply forward peaking distribution for the $(0_0, 1)^{\neq}$ pair generally suggests time-delay reaction mechanisms[33] and most likely, in the present case, a short-lived complex pathway as the $(0_0, 1)$ pair from ground-state reaction.[23] Similar measurements were performed at different E_c, and four of them are presented in Fig. 2. The overall behaviors are quite similar, except the subtle variation

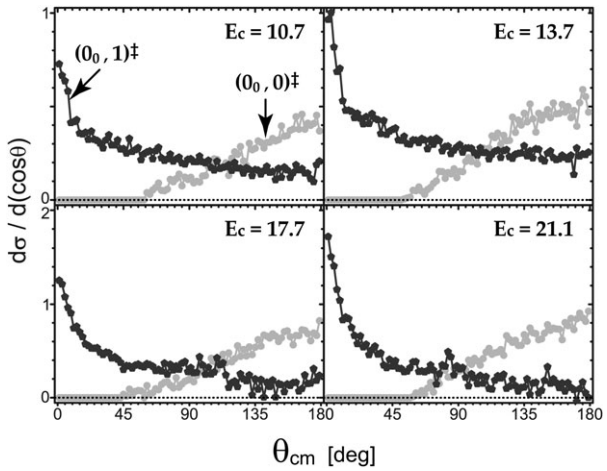

Fig. 2 As Fig. 1(d), except at four different collision energies, E_c in the unit of kJ mol^{-1}.

in the relative intensities of the sharp forward peak to the more broadly scattered component of the $(0_0, 1)^{\neq}$ pair. It is worth noting that these pair-correlated angular distributions bear a remarkable resemblance to the corresponding ones in the Cl + $CHD_3(v_1 = 1) \rightarrow CD_3(v = 0) + HCl(v' = 0,1)$ reaction.[11,32]

Integrating each distribution shown in Fig. 1 and 2 over all angles, weighted by the sinθ term for the solid-angle factor (where θ is the product-scattering angle), and accounting for only $\sim$19% of the CH_4 reactants being pumped, we deduced the normalized, pair-correlated integral cross section at each E_c. The reactive excitation function $\sigma_0(E_c)$ *i.e.*, the dependence of the integral cross section on E_c, of the ground-state reaction obtained from the IR-off images agreed with the previous report.[25] By measuring the relative cross section for $CH_4(v_3 = 1)$ to that for $CH_4(v = 0)$ at each E_c, the reactive excitation function $\sigma^{\neq}(E_c)$ of the Cl + $CH_4(v_3 = 1)$ reaction was then determined and presented in Fig. 3(a). As is seen, while the ground-state reaction displays a clear threshold around 10.5 kJ mol^{-1},[25] the stretch-excited reactivity remains significant over the E_c-range of this study. Plotted in Fig. 3(b) on logarithmic scale is the vibrational enhancement factor $(\sigma^{\neq}/\sigma_0)$ which, due to the threshold effect, increases sharply from less than 3 to about 60 with the decrease in E_c. At E_c = 15.5 kJ mol^{-1}, a vibrational enhancement factor of $\sim$10 is in reasonable agreement with the recent result of 13.4 by Zare and coworkers.[22] It is also worth noting that the E_c-dependence of the vibrational enhancement factor resembles that found previously for the Cl + $CHD_3(v_1 = 1)$ reaction,[11] except that the whole curve in the present case appears shifted downward by a factor of 1.4 $\pm$ 0.2. Clearly, the interpretation of the observed vibrational enhancement in reactivity goes beyond the simple collision-induced IVR mechanism,[7,18] in which the initially delocalized v_3-mode excitation will be transformed into a predominantly distal or unreactive local mode. It, thus, can't account for such a significant enhancement, unless subsequent nonadiabatic transitions occur between the two local modes.

The comparison of the two isotopic reactions is more striking in terms of pair-correlated vibration branching $\sigma_1^{\neq}/\sigma_0$, where $\sigma^{\neq} = \sigma_0^{\neq} + \sigma_1^{\neq}$ and $\sigma_i^{\neq}$ denotes the reactive

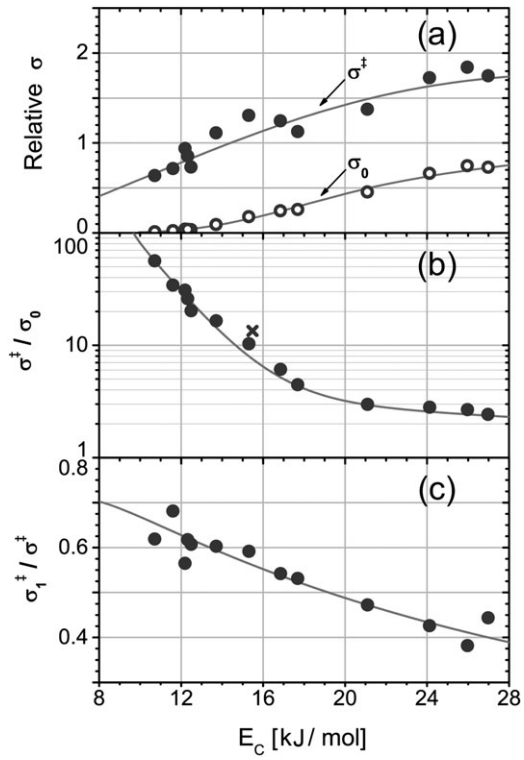

Fig. 3 (a) Normalized reactive excitation functions of the Cl + $CH_4(\nu) \rightarrow CH_3(\nu = 0) + HCl(\nu')$ reactions, with $\sigma^{\neq}$ and σ_0 denoting the reactive cross sections from the antisymmetric-stretch excited (ν_3 = 1) and ground-state (ν = 0) reactants, respectively. (b) The vibrational enhancement factors at fixed E_c. Also, shown by "×", for comparison is the recent measurement by Zare and coworkers (ref. 22) at E_c = 15.5 kJ mol^{-1}. (c) The vibrational branching fractions of the coincidently formed HCl(v' = 1) products from the Cl + $CH_4(\nu_3 = 1)$ reaction. Solid lines are visual guides.

cross section in forming the $CH_3(v = 0) + HCl(v' = i)$ product pair from the stretch-excited reactant. While the vibrational branching fraction for the Cl + $CHD_3(v_1 = 1) \rightarrow CD_3(v = 0) + HCl(v')$ reaction rises abruptly at energetic threshold and then remains roughly constant around 0.44,[11] the present reaction (Fig. 3(c)) displays a clear downward trend from about 0.65 at $E_c \sim$ 10 kJ mol^{-1} to 0.4 at $E_c \sim$ 28 kJ mol^{-1}.

Based on the vibrational mode correlation between the reactant and product pairs, we previously proposed a conceptual framework for understanding mode-specific reactivity.[11] In this framework, the reaction of Cl + $CHD_3(v_1 = 1)$ adiabatically correlates to the $CD_3(v = 0) + HCl(v' = 1)$ product pair. Hence, the formation of the ground-state product pair $CD_3(v = 0) + HCl(v' = 0)$, which correlates to the ground-state reactants, from the $CHD_3(v_1 = 1)$ reaction must involve vibrationally nonadiabatic transitions, in line with theoretical predictions of strong curvature couplings between the C–H stretching (v_1 = 1) mode and the reaction coordinate.[12–14] In other words, the curvature coupling of the C–H stretching mode induces a bifurcation of the reactive fluxes into an adiabatic and a nonadiabatic pathways leading to the observed $(0_0, 1)^{\neq}$ and $(0_0, 0)^{\neq}$ product pairs, respectively.[11] Nearly constant vibration branching fraction $\sigma_1^{\neq}/\sigma^{\neq} \cong 0.44$

over the energy range of 10–50 kJ mol^{-1} will then suggest that the curvature coupling is not a strong function of E_c.

By contrast, the present reaction of Cl-atom with a triply degenerate, antisymmetrically stretch-excited $CH_4(v_3 = 1)$ correlates adiabatically to the stretch-excited $CH_3(v_1 = 1$ and $v_3 = 1)$ and $HCl(v' = 0)$ product pair.[23] *Ab initio* calculations showed that the generalized vibration frequencies of that correlation are nearly invariant along the reaction coordinate.[12,13] It implies that the reactant v_3-mode is a spectator; thus, no vibrational enhancement is anticipated for that adiabatic-correlated product channel. Here, the probed product pair $CH_3(v = 0)$ + $HCl(v' = 1)$ correlates instead to the Cl + $CH_4(v_1 = 1)$ reactant pair, for which an adiabatic potential well is present in the transition state region.[23] As the Cl-atom approaches the IR-excited $CH_4(v_3 = 1)$, the intermolecular interactions will perturb the vibrational motions of an isolated molecule. As such, the laser-prepared eigenstate evolves into a superposition state in the basis of vibrational eigenstates for the Cl–CH_4 colliding pair, and mode-mixing ensues. In other words, the formations of $(0_0, 1)^{\neq}$ and $(0_0, 0)^{\neq}$ product pairs from the v_3-excited reactant are conceivably initiated by the v_1/v_3 mode-mixing in the entrance valley of the Cl + CH_4 reaction, as previously suggested.[6,7] This collision-induced mode mixing in the entrance valley is expected to be facile for both the proximity of the vibrationally adiabatic surfaces of the two stretches and long interaction time of heavy reactants' slow motions. Since the excited v_1-adiabatic pathway has a lower activation barrier[23] and been predicted theoretically more reactive,[12–18] a substantial mixing of the v_1-character into the initially prepared v_3-excited reactant could then result in the rate promotion of the Cl + $CH_4(v_3 = 1)$ reaction as seen in Fig. 3(b).

However, the observation of a relatively high branching fraction in forming the $(0_0, 1)^{\neq}$ pair near the energetic threshold followed by a rapid decline with the increase in E_c (Fig. 3(c)) is perplexing and in sharp contrast to the behaviors observed in the Cl + $CHD_3(v_1 = 1)$ reaction.[11] This unexpected result suggests that the reactivity of $CH_4(v_3 = 1)$ leading to different product pairs is probably more than just the v_1/v_3 mode mixing; otherwise, an E_c-independent vibration branching as that from the C–H stretch-excited CHD_3 reaction[11] would have been observed. Additional factors must be involved in differentiating the vibrational branching behaviors of the two stretch-excited isotope reactions.

It is also instructive to compare the HCl vibrational branching fractions from the stretch-excited and ground-state reactants of the two isotopic reactions. Despite the different dependences on E_c as just discussed, the correlated vibration branchings from both stretch-excited reactants are more than one order-of-magnitude larger than the respective, translationally hot ground-state reactions with equivalent amount of total energy.[11,23] For the ground-state reaction, based on the observed characteristic pattern on the $d\sigma/d(\cos\theta) - \theta - E_c$ plot of the $(0_0, 1)$ product pair, a resonance-complex reaction mechanism was proposed for its formation.[23] And the pathway leading to the resonant complex formation is induced by a translation-to-vibration ($T \rightarrow V$) energy transfer process in the entrance valley.[23] If the behavior of $CH_4(v_3 = 1)$ reactivity is indeed mediated in part (*i.e.*, although it can't be the full story as aforementioned) by the v_1/v_3 mode-mixing, then the large disparity in vibrational branching fractions between the two methane states (the antisymmetric stretch-excited and ground states) may reflect the relative inefficiency of the T → V energy transfer compared to the collision-induced mode mixing in the entrance valley.

In summary, product pair-correlation was measured, using a time-sliced velocity-map imaging technique, for the Cl + $CH_4(v_3 = 1) \rightarrow CH_3(v = 0)$ + $HCl(v' = 0,1)$ reaction under crossed-beam conditions. Over the energy range of this study, significant vibrational enhancements in reactivity were observed. Its energy dependence is nearly the same as that for the isotopically analogous reaction of Cl + $CHD_3(v_1 = 1) \rightarrow CD_3(v = 0)$ + $HCl(v' = 0,1)$ except an overall downward shift by a factor of 1.4. The correlated HCl vibrational branching fraction $\sigma_1^{\neq}/\sigma^{\neq}$, however, exhibits an intriguing E_c-dependency, in sharp contrast to the E_c-independent branching for the Cl + $CHD_3(v_1 = 1)$ reaction. The origin of this difference is not fully understood at present. Further study to unveil the nature of state mixings is in progress.

Acknowledgements

We thank Dr B. Zhang for his helps in the initial phase of this project. This work was financially supported by National Science Council of Taiwan, Academia Sinica, and the Air Force Office of Scientific Research (AOARD-07-4005).

References

1. F. F. Crim, *Acc. Chem. Res.*, 1999, **32**, 877.
2. R. N. Zare, *Science*, 1998, **279**, 1875.
3. A. Sinha, M. C. Hsaio and F. F. Crim, *J. Chem. Phys.*, 1990, **92**, 6333.
4. M. J. Bronikowski, W. R. Simpson, B. Girard and R. N. Zare, *J. Chem. Phys.*, 1991, **95**, 8647.
5. (*a*) W. R. Simpson, A. J. Orr-Ewing and R. N. Zare, *Chem. Phys. Lett.*, 1993, **212**, 163; (*b*) W. R. Simpson, T. P. Rakitzis, S. A. Kandel, A. J. Orr-Ewing and R. N. Zare, *J. Chem. Phys.*, 1995, **103**, 7313.
6. H. A. Bechtel, J. P. Camden, D. J. A. Brown and R. N. Zare, *J. Chem. Phys.*, 2004, **120**, 5096.
7. S. Yoon, S. Henton, A. N. Zivkovic and F. F. Crim, *J. Chem. Phys.*, 2002, **116**, 10744.
8. S. Yoon, R. J. Holiday and F. F. Crim, *J. Phys. Chem. B*, 2005, **109**, 8388.
9. S. Yoon, R. J. Holiday, E. L. Sibert III and F. F. Crim, *J. Chem. Phys.*, 2003, **119**, 9568.
10. J. Zhou, J. J. Lin, B. Zhang and K. Liu, *J. Phys. Chem. A*, 2004, **108**, 7832.
11. S. Yan, Y. T. Wu, B. Zhang, X. Yue and K. Liu, *Science*, 2007, **316**, 1723.
12. W. T. Duncan and T. N. Truong, *J. Chem. Phys.*, 1995, **103**, 9642.
13. J. C. Corchado, D. G. Truhlar and J. Espinosa-Garcia, *J. Chem. Phys.*, 2000, **112**, 9397.
14. J. Espinosa-Garcia, *J. Phys. Chem. A*, 2007, **111**, 5792 and 9654.
15. J. Sanson, J. C. Corchado, C. Rangel and J. Espinosa-Garcia, *J. Phys. Chem. A*, 2006, **110**, 9568.
16. R. Martinez, M. Gonzalez, P. Defazio and C. Petrongolo, *J. Chem. Phys.*, 2007, **127**, 104302.
17. G. C. Schatz, *J. Chem. Phys.*, 1979, **71**, 542.
18. J. R. Fair, D. Schaefer, R. Kosloff and D. J. Nesbitt, *J. Chem. Phys.*, 2002, **116**, 1406.
19. L. Halonen, *J. Chem. Phys.*, 1997, **106**, 831.
20. S. Carter, H. S. Shnider and J. M. Bowman, *J. Chem. Phys.*, 1999, **110**, 8417.
21. W. R. Simpson, T. P. Rakitzis, S. A. Kandel, T. Lev- On and R. N. Zare, *J. Phys. Chem.*, 1996, **100**, 7938.

22. R. N. Zare and D. J. A. Brown, private communications D. J. A. Brown, PhD Dissertation, Stanford University, 2007.
23. B. Zhang and K. Liu, *J. Chem. Phys*., 2005, **122**, 101102.
24. X. Wang, M. Ben-Nun and R. D. Levine, *Chem. Phys*., 1995, **197**, 1.
25. J. Zhou, B. Zhang, J. J. Lin and K. Liu, *Mol. Phys*., 2005, **103**, 1757.
26. K. Liu, *J. Chem. Phys*., 2006, **125**, 132307; K. Liu, *Annu. Rev. Phys. Chem*., 2001, **52**, 139.
27. A. S. Pine, *J. Opt. Soc. Am*., 1976, **66**, 97.
28. W. Shiu, J. J. Lin and K. Liu, *Phys. Rev. Lett*., 2004, **92**, 103201.
29. J. J. Lin, J. Zhou, W. Shiu and K. Liu, *Rev. Sci. Instrum*., 2003, **74**, 2495.
30. J. J. Lin, J. Zhou, W. Shiu and K. Liu, *Science*, 2003, **300**, 966.
31. K. Liu, *Phys. Chem. Chem. Phys*., 2007, **9**, 17.
32. S. Yan, Y. T. Wu and K. Liu, *Phys. Chem. Chem. Phys*., 2007, **9**, 250.
33. J. Zhou, J. J. Lin, W. Shiu and K. Liu, *J. Chem. Phys*., 2003, **119**, 4997.

Imaging the pair-correlated dynamics and isotope effects of the $Cl+CH_2D_2$ reaction

Yen-Tien Wu and Kopin Liu[a)]
Institute of Atomic and Molecular Sciences (IAMS), Academia Sinica, P. O. Box 23-166, Taipei 10617, Taiwan

(Received 14 August 2008; accepted 12 September 2008; published online 16 October 2008)

By using a time-sliced (ion) velocity-imaging technique, the title reaction was investigated to interrogate the pair-correlated dynamics of HCl (DCl) in concomitance with the CHD_2 or CHD_2 ground-state product under the crossed-beam conditions. Product pair-correlated excitation functions, vibrational branching ratios, and angular distributions were obtained over a wide range of collision energies, from 2 to 22 kcal/mol. Two distinct reaction mechanisms were uncovered. Both the dominant ground-state reaction of $Cl+CH_2D_2(v=0)\rightarrow HCl(v=0)/DCl(v=0)+CHD_2(0_0)/CH_2D(0_0)$ and the reaction forming the same product pairs from bend-excited CH_2D_2 reactants proceed through direct mechanisms, which shift from a rebound dynamics near thresholds to a peripheral dynamics at higher E_c. Reactivity of forming the $HCl(v=1)/DCl(v=1,2)+CHD_2(0_0)/CH_2D(0_0)$ product pairs from ground-state reactants is small, yet shows dynamics pattern characteristics of a resonant reaction pathway. Significant spin-orbit reactivity of $Cl^*(^2P_{1/2})$ was discovered, and its mechanism appears to be also mediated by the resonant reaction pathway. Comparing the dynamical attributes of the H- and D-atom transfer channels, remarkable isotope effects are found—in line with the previous findings in the $Cl+CH_4/CD_4$ and $Cl+CHD_3$ reactions. © *2008 American Institute of Physics*. [DOI: 10.1063/1.2993264]

I. INTRODUCTION

The hydrogen abstraction reaction of the chlorine atom with methane plays a crucial role in the ozone production/depletion cycle in the stratosphere[1] and has been the subject of intense investigations, both experimentally[2] and theoretically,[3] over the past decades. More recently, this reaction has been under a more detailed dynamical scrutiny and is becoming a paradigm for fundamental understanding of polyatomic reaction dynamics.[4–6] In particular, ample evidence has been gathered, demonstrating the dominance of the peripheral reaction mechanism.[7–10] A peripheral mechanism occurs for reactions proceeding preferentially with large impact-parameter (b) collisions, giving rise to a skewed opacity function $P(b)$ strongly in favor of higher b values.[7] In order for a large impact-parameter trajectory to be reactive, the attacking Cl atom needs not only to move under a central potential but also to experience an attraction to the abstracted peripheral hydrogen atom.

One of the experimental manifestations of peripheral dynamics appears as the unusual shape of the product angular distribution.[7–11] Although the distribution is mainly backward scattered near the reaction threshold for a limited range of small impact-parameter collisions to reaction, as the collision energy E_c increases, it shifts progressively toward sideways/forward with a characteristic sharp cutoff in angles against the formation of small scattering-angle products. In the primitive line-of-center model, this sharp cutoff originates from the requirement that only those collisions with sufficient line-of-center energy to surmount the centrifugal-shifted barrier can react,[8] and the characteristic angular distribution with predominant sideways peaking arises from the one-to-one correspondence between the scattering angle and the impact parameter of the skewed opacity function $P(b)$ in a direct collision.[8,11] Such behaviors, a rebound mechanism near the threshold and shifting to peripheral dynamics at higher E_c, are nicely borne out in recent crossed-beam studies on $Cl+CH_4$ and CD_4,[8,9] as well as on $Cl+CHD_3$.[10] Moreover, closer comparisons of the H- and D-atom abstraction channels revealed a striking isotope effect. At $E_c \sim 7$ kcal/mol, for example, while the angular distribution of $Cl+CD_4$ reaction peaks near 90° with an intensity ratio of $I(180°)/I(90°)\sim 0.7$, that of $Cl+CH_4$ is so sharply peaked at 60° that more than 90% of product fluxes are confined within the angular range of 30°–90° with a ratio of $I(180°)/I(60°)\sim 0.07$![8] The Born–Oppenheimer potential energy surfaces of the two isotopic reactions are identical; yet, their product angular distributions differ so dramatically. Both the zero-point energy and the effect of tunneling through the centrifugal-shifted barrier to reaction are in favor of H-atom abstraction channel, which have been proposed to qualitatively account for the striking isotope difference in angular distributions by enhancing the characters of peripheral dynamics when a H atom is abstracted.[8] Replacing the tetrahedral CH_4/CD_4 reactants by CH_2D_2 breaks the reaction symmetry, as such the Cl atom will feel different peripheral interactions as the H atom or D atom is attacked, offering a more stringent test of the peripheral mechanism.

Also closely related to the present study are the two remarkable reports on the bond and mode selectivity of the title reaction with vibrationally excited CH_2D_2 by Zare and

[a)]Electronic mail: kpliu@po.iams.sinica.edu.tw.

co-workers.[12,13] They found that excitation of the first C–H overtone of CH_2D_2 promotes only the H-atom abstraction reaction, and excitation of the first C–D overtone of CH_2D_2 leads preferentially to the C–D bond cleavage. In addition, excitation of different modes, either two quanta in one C–H oscillator or a local mode containing one quantum each in two C–H oscillators, produces vastly different product states and angular distributions. The major findings of these bond and mode-selective investigations can be summarized by an intuitively simple spectator model,[12,13] in which the Cl atom interacts with the single C–H oscillator and the remainder of the methane molecule does not participate in the reaction.

To complement the previous studies and to shed more light into the fascinating mode and bond selectivity in general, we report here an extensive study on reactions of $Cl+CH_2D_2 \rightarrow CHD_2+HCl$ and CH_2D+DCl. Both the integral and differential cross sections were measured over a wide range of collision energies, ~2–22 kcal/mol. In addition, the reactivity of the spin-orbit excited $Cl^*(^2P_{1/2})$ toward $CH_2D_2(v=0)$ and that of bend/torsion-excited CH_2D_2 with $Cl(^2P_{1/3})$ are characterized. This rather extensive data set then lays a firm foundation for understanding an on-going study in this laboratory on the mode-selective reactivity with one quantum excitation of two different CH_2-stretching modes (symmetric $v_1=1$ or antisymmetric $v_6=1$) in $Cl+CH_2D_2$.[14]

II. EXPERIMENT

The experiments were carried out using the crossed-beam apparatus described in detail elsewhere.[8–10,15] In brief, a pulsed high-voltage discharge method was used to generate the Cl-atom beam (3.5% Cl_2 seeded in helium at 6 atm of total pressure). A diluted CH_2D_2 (~18% CH_2D_2 seeded in H_2 at 6 atm) from an *E-L* valve[16] was used to cover the entire E_c-range of this study, ~2 to greater than 20 kcal/mol. The reaction products, CHD_2 and CH_2D, were probed by (2+1) resonance-enhanced multiphoton ionization (REMPI) process[17,18] using a time-sliced ion velocity-imaging technique to interrogate the product-pair-correlated information.[15,19] REMPI spectra of both reaction products indicated predominant formation of the vibrational ground state; thus, this report will focus on the pair-correlated dynamics with respect to the $CHD_2(v=0)$ and $CH_2D(v=0)$ products. Experiments on probing the vibrationally excited methyl products are in progress; the results will be reported in the future.

At a given collision energy, the time-sliced image was acquired with the probe laser frequency fixed at the peak of the 0_0^0 *Q*-head of the $X\,^2B_1 \rightarrow 3p^2B_1$ transition, namely, at the two-photon frequencies (in vacuum) of 59 921 cm^{-1} for CHD_2 and of 59 940 cm^{-1} for CH_2D.[17,18] The observed *Q*-head is substantially broader than the probe laser bandwidth. Previous investigations from this laboratory showed some subtle differences in pair-correlated information from two alternative modes of operation, that is, either by fixing the probe laser near the peak of the *Q*-head or by scanning the laser frequency back and forth across the *Q*-head while acquiring the image.[20,21] The observed differences have also been demonstrated to originate from a surprisingly sensitive dependence of the vibrational branching ratio of the coproducts [HCl (Ref. 21) or HF (Ref. 20)] on the probed rotational *N*-states of the methyl products. Although the vibrationally correlated information arguably could be less biased toward the probed *N*-states by scanning the laser frequency, this mode of operation generally blurs the velocity-mapped image resolution. Because we were also interested in the reactivity of $Cl^*(^2P_{1/2})$ and of the bend-excited CH_2D_2, for which the velocity resolution is of prime concern, we chose to fix the laser frequency near the peak of *Q*-head. Thus, the pair-correlated information in this report refers to that with respect to the $v=0$, low *N* states of the methyl products.[20,21]

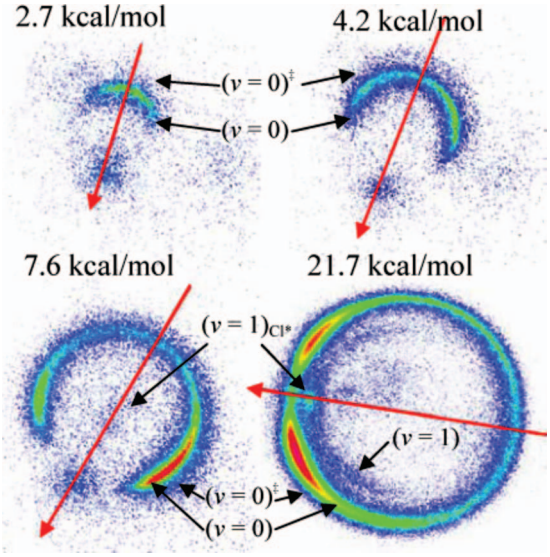

FIG. 1. (Color) Representative time-sliced raw images of $CHD_2(0_0)$ products at four different collision energies. The state labelings $(v=0)$, $(v=1)$, $(v=0)^{\ddagger}$, and $(v=1)^*$ correspond to the correlated HCl vibration states from the reactions of (1) $Cl+CH_2D_2(0_0) \rightarrow CHD_2(0_0)+HCl(v=0)$, (2) $Cl+CH_2D_2(0_0) \rightarrow CHD_2(0_0)+HCl(v=1)$, (3) $Cl+CH_2D_2(v_{bend}=1) \rightarrow CHD_2(0_0)+HCl(v=0)$, and (4) $Cl^*(^2P_{1/2})+CH_2D_2(0_0) \rightarrow CHD_2(0_0)+HCl(v=1)$, respectively.

Depending on the signal strength, each time-sliced image was taken at 20 Hz for 1–4 h, accumulating 1×10^5 to 6×10^5 total events. To normalize the images at different collision energies for obtaining the reactive excitation functions, the procedure described elsewhere[22] was followed in separate measurements. Relative detection sensitivities of probing the 0_0^0 bands of CHD_2 and CH_2D are yet to be calibrated. Hence, the comparison of the relative cross sections of the two isotope channels was merely based on the relative signal strengths under otherwise identical experimental conditions.

III. RAW IMAGES AND PAIR-CORRELATED ANGULAR DISTRIBUTIONS

Figure 1 presents typical raw images of the $CHD_2(v=0)$ product at four different collision energies, and similarly, Fig. 2 for the $CH_2D(v=0)$ product. The energetics of the reaction are well established: $\Delta H_{rx}=1.5$ and 1.9 kcal/mol for the $HCl+CHD_2$ and $DCl+CH_2D$ isotope channels, respectively; so as the vibrational energies of HCl (8.24 kcal/mol for $v=1$) and DCl (5.79 and 11.79 kcal/mol for $v=1$ and

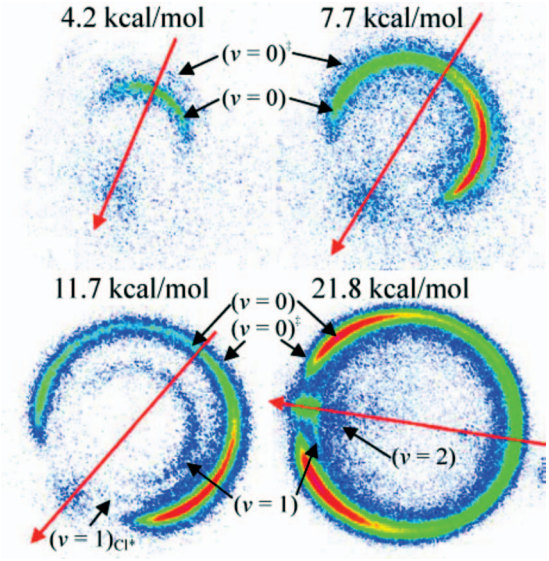

FIG. 2. (Color) Similar to Fig. 1, but for the $CH_2D(0_0)+DCl$ product channel.

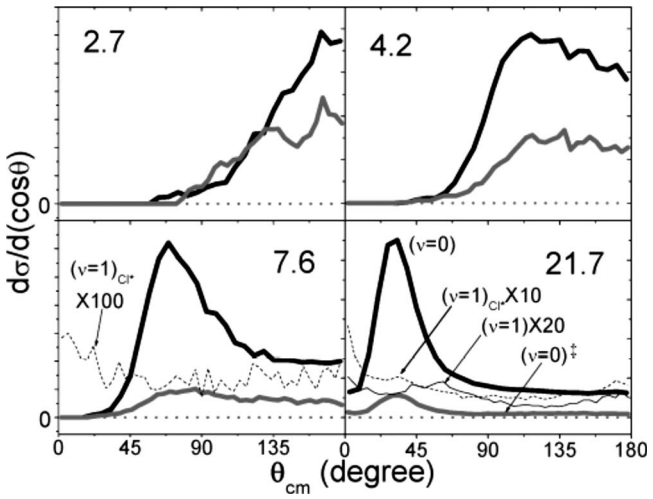

FIG. 3. The pair-correlated angular distributions of the $Cl+CH_2D_2 \rightarrow CHD_2+HCl$ reactions derived from the four images shown in Fig. 1. The line symbols are the same for all four panels with the state labels (right-bottom panel) as Fig. 1. For clarity, the intensities of the minor channels are amplified.

2, respectively) and the spin-orbit energy of 2.52 kcal/mol for $Cl^*(^2P_{1/2})$. Hence, on energetic grounds, all ringlike features on the image can readily be identified and assigned to the vibrational states of the coproducts from different reactant states as labeled in the figure and explained in the caption. The red line in each image indicates the relative velocity vector in the center-of-mass (c.m.) frame with the arrow pointing to the 0°, which is defined as the direction of the CH_2D_2 beam in the c.m. frame. As can be seen, the angular distribution of the CHD_2 or CH_2D radical coincidently formed with $HCl(v=0)$ or $DCl(v=0)$, which is the most prominent feature in Fig. 1 or Fig. 2, evolves from backward near threshold to sideways and then into forward hemisphere at successively higher E_c. Such a systematic angular evolution with E_c appears at a faster pace for the CHD_2+HCl product channel than for CH_2D+DCl.

The raw images shown in Figs. 1 and 2 do not possess the cylindrical symmetry around the relative velocity axis because of the nonuniform detection dependency on the product laboratory velocity.[15,23] After correcting for the density-to-flux transformation,[15] quantitative angular distribution of each distinct ring can then be deduced. The results of such image analysis are presented in Figs. 3 and 4 for Figs. 1 and 2, respectively. A few remarks are in order. First, for the dominant product states labeled $(v=0)$, the general trends of the angular distributions of the two isotopic product channels are alike except the different rates of angular evolutions on E_c, as alluded to above. A closer comparison reveals some subtle, perhaps significant, differences between the two product channels. At $E_c \sim 21.7$ kcal/mol, the $HCl+CHD_2$ channel indicates finite, albeit small, fluxes near 0°, which is evident from the ring closure in Fig. 1, whereas the flux along the forward direction is negligibly small in the $DCl+CH_2D$ channel. In addition, the ratio of the peak intensity to the flux at 180° is clearly larger for $HCl+CHD_2$ than that for $DCl+CH_2D$. Similar behavior is seen from the comparison of $HCl+CHD_2$ at 7.6 kcal/mol to $DCl+CH_2D$ at 11.7 kcal/mol, even though the former is at lower E_c. The disparity in the sharpness of angular peaks of the two isotope channels is reminiscent of the previous findings of the *H*-versus D-atom abstractions from the $Cl+CH_4$ and CD_4 reactions.[8]

Second, a few minor image features are worth noting. The angular distributions of product ground-state pairs from the bend-excited reaction (see Sec. IV) resemble the respective ground-state reactions (see Figs. 3 and 4). It implies that the bend-excited reaction follows nearly the same pathway as the ground-state reaction. Similar results were found previously in reactions of other isotopomers.[24,25] Since the bend-excited reactants correlate adiabatically to the bend-excited methyl products,[25,26] vibrationally nonadiabatic transitions must occur at the entrance channel in order for bend-state reactions to proceed over the ground-state reaction pathway by funneling the bending energies into the product translational and rotational energies (i.e., acting as a transitional mode).[26] The same interpretation was proposed previously for the other isotopically analogous reactions.[25,26]

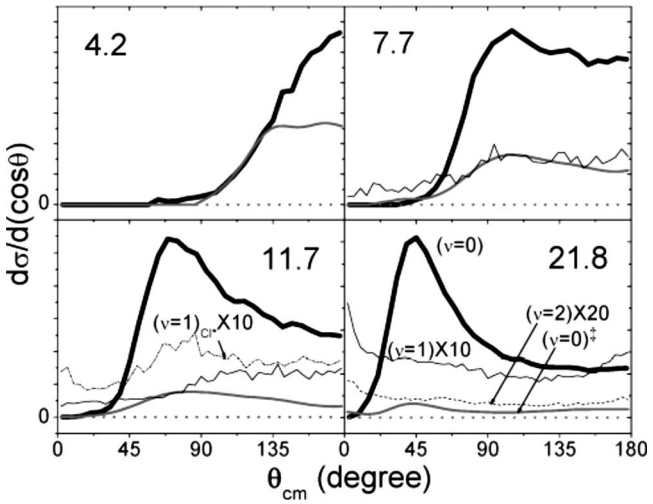

FIG. 4. Similar to Fig. 3, the pair-correlated angular distributions of the $Cl+CH_2D_2 \rightarrow CH_2D+DCl$ reactions derived from the four images shown in Fig. 2.

As to the vibrationally excited HCl($v=1$) from ground-state reactants (the thin solid lines in Fig. 3), the correlated angular distributions are distinctly different, featuring a clear forward and a weak yet discernible backward peaks superimposed on a nearly isotopic component—in analogy to the other isotopomers.[9,25] In general, such an angular distribution is suggestive of some time-delay reaction mechanisms,[27–31] and most likely, in the present case, a short-lived resonant complex pathway.[9,25,26] The formation of DCl($v=1$) from the ground-state reactants, however, exhibits a rather different angular distribution (Fig. 4), which appears to constitute two components. At low E_c, the distribution resembles the corresponding ground-state product pair except a persistent forward component; at high E_c, it turns into a forward-backward peaking distribution in analogy to the HCl($v=1$) product. In other words, two distinct mechanisms of the direct and the resonant reaction pathways dominate over the low and high E_c regimes, respectively, in forming the DCl($v=1$)+$CH_2D(0_0)$ product pair. The angular distribution for the DCl($v=2$) coproduct, which is accessible only at $E_c > 13.7$ kcal/mol, is similar to DCl($v=1$) at high E_c, i.e., a forward-backward peaking one.

The most intriguing finding for the reaction with spin-orbit excited $Cl^*(^2P_{1/2})$ is the clear formation of the HCl/DCl coproducts with one quantum of vibrational excitation. The correlated angular distribution of $HCl(v=1)_{Cl^*}$ is characterized by the distinct forward-backward asymmetric peaks (the dotted lines in Fig. 3), whereas that of $DCl(v=1)_{Cl^*}$ exhibits additional sideways feature that resembles the ground-state pair from the peripheral pathway (Fig. 4). In other words, the observed angular distribution suggests that the $Cl^*(^2P_{1/2})+CH_2D_2(v=0)\rightarrow CHD_2(0_0)+HCl(v=1)$ reaction proceeds mainly via the resonant complex pathway. However, both the resonant complex and peripheral pathways contribute to the formation of $CH_2D(0_0)$+DCl($v=1$).

IV. REACTIVITY OF BEND-EXCITED CH_2D_2

The above assignment of a ringlike feature to the $(0_0,0)^{\neq}$ product pair from the reaction with bend-excited CH_2D_2 needs further clarification. The reactant CH_2D_2 has nine vibrational degrees of freedom; five of them are low-frequency modes (i.e., <1500 cm^{-1}): CD_2 scissor (1033 cm^{-1}), CH_2 rock (1090 cm^{-1}), CH_2 wag (1234 cm^{-1}), CH_2 twist (1333 cm^{-1}), and CH_2 scissor (1436 cm^{-1}).[32] The first two modes contain merely ~0.5 kcal/mol more energy than the spin-orbit excited $Cl(^2P_{1/2})$ atom (852 cm^{-1}). The latter must also be present in our discharge-generated beam, as evidenced by the $(0_0,1)_{Cl^*}$ feature as well by the previous finding in $Cl+CH_4$.[9] Therefore, energetic argument alone is not sufficient for an unambiguous assignment. The unequivocal evidence came from the separate experiment of using a heated CH_2D_2 pulsed valve, as first demonstrated in the studies of $Cl+CH_4/CD_4$ (Ref. 24) and $O(^3P)+CD_4/CHD_3$ (Ref. 33) reactions.

Shown in Fig. 5 are the results from a back-to-back experiment of the HCl(v)+$CHD_2(0_0)$ channel, for which the CH_2D_2-valve temperature was varied. The molecular-beam intersection angles were adjusted slightly so that the collisional energies from different source temperatures remained about the same, $E_c \sim 5.8$ kcal/mol. Even a casual inspection of the raw image reveals a significant enhancement in the $(v=0)^{\neq}$ feature at higher temperature (439 K). More quantitative comparison is demonstrated from the fully analyzed product speed distribution $P(u)$,[15] which shows two well-resolved peaks (the lower panel of Fig. 5). For ready comparison, the $P(u)$ distributions from the two source temperatures are normalized by the peak height of the slow component, which is ascribed to $Cl+CH_2D_2(v=0)\rightarrow HCl(v=0)+CHD_2(0_0)$. As is seen, the $P(u)$ distribution for 439 K displays a more intense fast component with the intensity ratio of the fast-to-slow components increasing from ~9% at 320 K to ~32% at 439 K. Because the Cl beam was kept the same, this difference by heating the CH_2D_2 valve provided a compelling evidence for the assignment of the fast component mainly to the $(0,0_0)^{\neq}$ product pair from the reaction with thermally excited CH_2D_2.

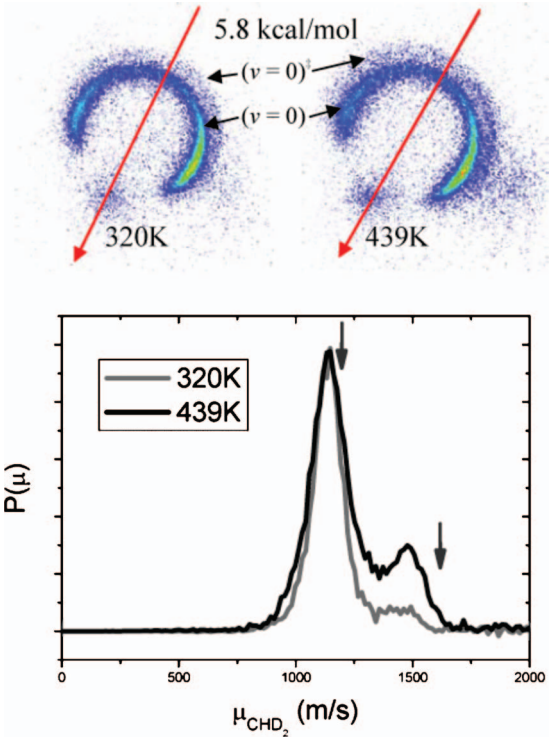

FIG. 5. (Color) Effect of low-lying hot bands of CH_2D_2 reactants on the observed images. The upper panels display the $CHD_2(0_0)$ product images at two different CH_2D_2 pulsed valve temperatures. The molecular-beam intersection angles were adjusted slightly so that the two images were acquired at the same $E_c \sim 5.8$ kcal/mol. The analysis of product speed distributions are presented in the lower panel. The two vertical arrows mark the maximal speeds from reactions with the ground-state and bend-excited reactants, respectively. For ready comparison, the intensities of two distributions are normalized by the peaks from the ground-state reaction (the slow component); significantly enhanced faster component at higher temperature is vividly displayed.

Previous studies on $Cl+CH_4/CD_4$ reactions demonstrated that although supersonic expansion yielded a translationally and rotationally cold (~5–10 K) methane beam, the low-lying vibration manifolds remain, by and large, thermally populated.[24] Assuming that the similar situation holds for the present CH_2D_2 beam, one can then estimate the reac-

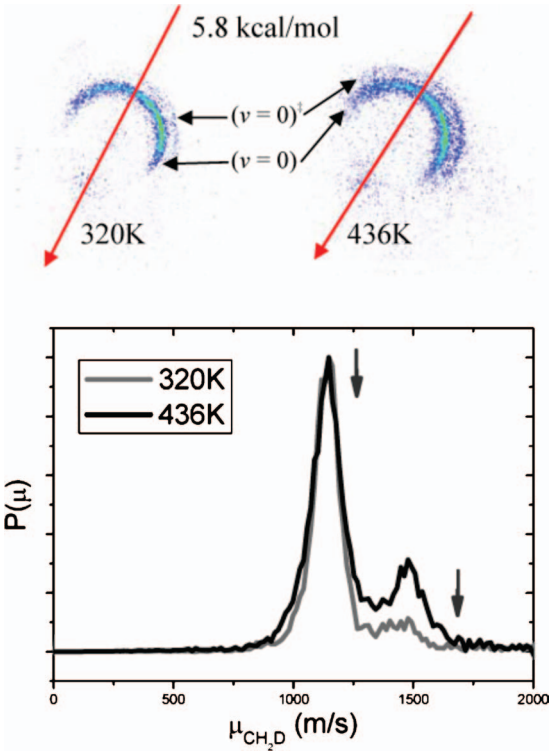

FIG. 6. (Color) Same as Fig. 5, but for the $CH_2D(0_0)+DCl$ product channel.

tivity of bend-excited reactants. The above fast-to-slow ratio corresponds to $\Sigma_i n_i \sigma_i^{\neq}/n_0\sigma_0$ with n_i denoting the population of the vibrationally excited state i of CH_2D_2 in the beam and $\sigma_i^{\neq}$ being the corresponding reaction cross section (the subscript "0" indicates the vibrational ground-state reactant). Since the thermally populated vibration manifolds follow the Boltzmann distribution (i.e., without state selection) and, energetically, the $P(u)$ distribution of the fast component rules out the contributions from higher-lying vibration levels, therefore only the five low-frequency modes need to be considered. We further approximated $\Sigma_i n_i \sigma_i^{\neq}/n_0\sigma_0$ as $\sigma^{\neq}\Sigma_i n_i/n_0\sigma_0$, with $\sigma^{\neq}$ representing the average cross section over those five modes. The Boltzmann factors $\Sigma_i n_i/n_0$ at 320 and 439 K are 0.025 and 0.102, respectively. Hence, the estimated vibrational enhancement factors $\sigma^{\neq}/\sigma_0$ are 3.6 (or 0.09/0.025) and 3.1 (or 0.32/0.102) from the analysis of the data at two temperatures. It is gratifying to note the self-consistency of the two estimated enhancement factors, which strongly suggests that, within our experimental uncertainties, the contribution of $Cl^*+CH_2D_2(v=0)$ to the formation of $HCl(v=0)+CHD_2(0_0)$ is relatively minor at this collision energy.

Similarly, Fig. 6 presents the images and the $P(u)$ distributions for the other isotope channel, $DCl+CH_2D$. The ratios of fast-to-slow components are ~8% and ~30% at 320 and 436 K, respectively, which, in turn, yield the respective $\sigma^{\neq}/\sigma_0 \sim 3.2$ and ~3.0 for the bend-excited enhancement factor at $E_c \sim 5.8$ kcal/mol; again, the agreement was quite reasonable. It is interesting to note that the vibrational enhancement factor of ~3 for bend-excited CH_2D_2 in both isotope channels is virtually the same as the factors obtained for the bend-excited $Cl+CH_4/CD_4$ (Refs. 24 and 34) and CHD_3 (Ref. 25) reactions.

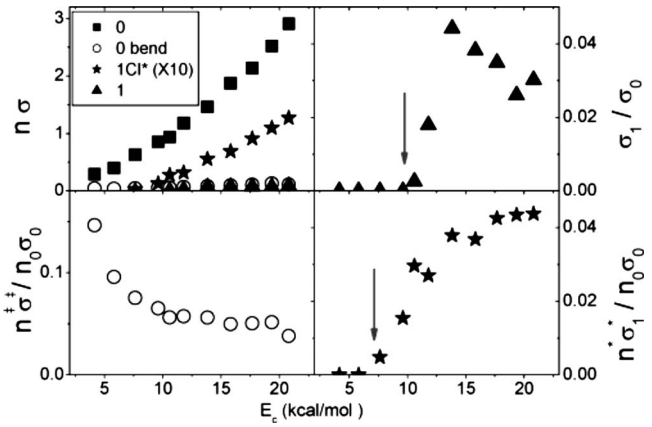

FIG. 7. The relative reactivity of the four state-to-state reactions listed in the caption of Fig. 1 when probing the $CHD_2(0_0)$ products. The left-top panel shows the relative excitation functions weighed by the respective reactant-state concentrations. The remaining three panels present the reactivity ratios to the dominant ground-state reaction cross section σ_0. To obtain the relative cross section of bend-excited reactants, $\sigma^{\neq}/\sigma_0$, the ordinate of the left-bottom panel should be divided by $n^{\neq}/n_0$, which is about 0.025 at the CH_2D_2 source temperature of 320 K. The vertical arrows in two right panels indicate the respective energetic thresholds of the two reaction channels.

V. CORRELATED EXCITATION FUNCTIONS AND RELATIVE REACTIVITY

After normalizing each individual methyl product image taken at different collision energies and correcting for the density-to-flux transformation, the energy dependence of reactive fluxes on the respective product-pair channels can then be deduced.[22] The resultant state-to-state excitation functions for the $HCl+CHD_2$ channel are presented in Fig. 7. As discussed above, four pair-correlated reaction channels were identified from the product image of $CHD_2(0_0)$. In addition to the two product pairs $CHD_2(0_0)+HCl(v=0$ and $1)$ from the ground-state reaction, the contributions from the excited reactants, i.e., $Cl(^2P_{3/2})+CH_2D_2^{\neq}(\text{bend}) \rightarrow CHD_2(0_0)+HCl(v=0)$ and $Cl^*(^2P_{1/2})+CH_2D_2(v=0) \rightarrow CHD_2(0_0)+HCl(v=1)$, were observed and analyzed. The relative signal of the latter two obviously depends on the initial population (n) of the excited reactant state in the molecular beam. Hence, the excitation functions shown in Fig. 7 (left-top panel) are plotted as $n\sigma$. The other three panels display the respective E_c-dependences of the ratios of those minor image features on $n_0\sigma_0$ of the dominant reaction channel $Cl+CH_2D_2(v=0) \rightarrow CH_2D(0_0)+HCl(v=0)$.

Compared to the ground-state reaction, the $(0_0,0)^{\neq}$ product pair from the bend-excited reactants (Fig. 7, left-bottom panel) displays a monotonic decline with increasing E_c. The estimated $n^{\neq}/n_0$ is about 0.025 at CH_2D_2 source temperature of 320 K; thus, the ordinate for $\sigma^{\neq}/\sigma_0$ should be multiplied by 40, yielding a vibrational enhancement of at least a factor of 2. It is tempting to attribute this enhancement factor to the energetic effect in that whereas the ground-state reaction possesses a barrier to reaction, the bend-excited reactants contain, on average, additional ~3.5 kcal/mol of energy for reaction. If the initial bend excitation of CH_2D_2 is readily coupled to the reaction coordinate through curvature couplings before the transition state, the transfer of bending energy will then help surmount

the reaction barrier, promoting the reaction rate. Yet, the observed vibrational enhancement becomes more pronounced at lower E_c, which is in sharp contrast to the previous finding of a nearly E_c-independent enhancement (at low E_c) for bend-excited CHD_3 in the $Cl+CHD_3 \rightarrow CD_3(0_0)+HCl$ reaction.[25] The observation of different E_c-dependencies of bend-mode enhancements of two isotope reactants is puzzling, perhaps points to the subtle differences in the curvature couplings and/or the Coriolis interactions among the bending/torsional modes. Further investigation is warranted.

The concomitant HCl vibrational branching ratio σ_1/σ_0 from the ground-state reaction (Fig. 7, right-top panel, the vertical arrow indicates the energetic threshold) remains small even at higher E_c, implying that the reaction of ground-state reactants is, by and large, vibrationally adiabatic. Same conclusion was drawn in the previous studies of $Cl+CH_4$ (Ref. 9) and $Cl+CHD_3$.[25] As to the $CHD_2(0_0)+HCl(v=1)$ pair from the spin-orbit excited $Cl^*(^2P_{1/2})$ reaction (Fig. 7, right-bottom panel), the relative reactivity $n^*\sigma_1^*/n_0\sigma_0$ exhibits a threshold around $E_c=7.3$ kcal/mol, as anticipated on energetic ground (the arrow). The relative population of $Cl^*(^2P_{1/2})$ in the beam, n^*/n_0, was not measured in this study, but is expected to be less than 1/2 (i.e., the relative degeneracy factors of the excited $^2P_{1/2}$ to the ground $^2P_{3/2}$ states); otherwise, population inversion ensues from discharging Cl_2 in He. With this caveat, the relative reactivity of $Cl^*(^2P_{1/2})$ toward CH_2D_2 appears quite significant at higher collision energies, e.g., σ_1^*/σ_0 will approach 9% at $E_c \sim 20$ kcal/mol or likely higher if n^*/n_0 is significantly less than 1/2. Perhaps even more remarkable is the fact that the concomitant product state here refers to the vibrationally excited $HCl(v=1)$; no image feature can be unambiguously ascribed to the energetically more readily accessible $HCl(v=0)$ coproduct, as pointed out in Sec. IV. It is interesting to note that the formation of $Cl^*(^2P_{1/2})$ product from the reverse reaction of CH_3/CD_3+HCl at $E_c \sim 20$ kcal/mol was recently reported.[35–37] However, in that study the CH_3/CD_3 reactant was generated photolytically from CH_3I/CD_3I, thus containing a significant amount of internal energy, whereas the HCl reactant is mostly in the $v=0$ state. Because of the differences between the initially prepared reactant states of that study and the probed product states of this study, it is difficult to compare the two investigations.

Similar results for the other isotope channel CH_2D+DCl are presented in Fig. 8. For the bend-excited reaction (left-bottom panel), again the relative reactivity $n^{\neq}\sigma^{\neq}/n_0\sigma_0$ declines with the increase in E_c, and the estimated $\sigma^{\neq}/\sigma_0$ should be scaled up by ~40 to account for the small relative population of $n^{\neq}/n_0$ in the CH_2D_2 beam. Compared to the CHD_2+HCl channel, the vibrational enhancements from the bend-excited reactants are comparable except near the ground-state reaction thresholds. For reaction with ground-state reactants, the formation of $DCl(v=2)$ becomes energetically accessible at higher E_c. Indeed, both σ_1/σ_0 and σ_2/σ_0 become finite at the respective energetic thresholds (indicated by the arrows). Their combined reactivity, however, remains small with respect to the ground-state product pair. Thus, the reaction of the ground-state reactants for this isotope channel is also largely vibrationally adiabatic, although its adiabaticity does not appear as strong as the $HCl+CHD_2$ channel. Unfortunately, due to the beam background (in the forward direction) problem and the higher demand in image resolution for this isotope channel, only for a few images of CH_2D over a limited E_c range can the spin-orbit excited features be analyzed; thus, its excitation function cannot be reliably determined.

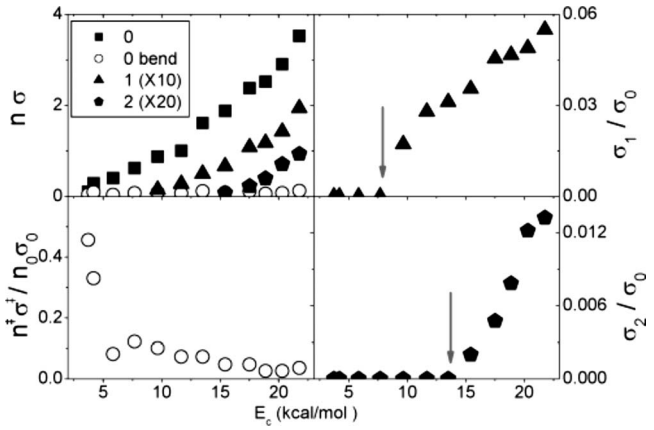

FIG. 8. Same as Fig. 7, but for the CH_2D+DCl product channels.

VI. E_c-EVOLUTION OF PAIR-CORRELATED ANGULAR DISTRIBUTIONS

By combining the pair-correlated excitation function presented in Sec. V and the angular distribution at each collisional energy as illustrated in Sec. III, a three-dimensional $d\sigma/d\Omega$-θ-E_c plot can be obtained.[6,19] Such a representation has proven to provide a global and illuminating view of the underlying reaction mechanism, in particular for the "discovery" of reactive resonances in the isotopically analogous reactions of $Cl+CH_4$ (Ref. 9) and CHD_3.[25] The results of the present four product pairs when $CHD_2(0_0)$ was probed are summarized in Fig. 9. As is seen, the patterns of $(v_{HCl}=0)$ and $(v_{HCl}=0)^{\neq}$ are alike, displaying a slowly evolving ridge structure that runs from a weak backward feature at low E_c toward an intense peak in the forward hemisphere at higher E_c. Virtually identical patterns were noted previously for the analogous product pairs from the $Cl+CH_4$ (Ref. 9) and CHD_3 reactions,[25] which were ascribed to a manifestation of a direct reaction governed by rebound mechanism near threshold and then shifting to peripheral dynamics at higher E_c.[8–10]

However, the two patterns shown in the lower panel are distinctly different. For $(v_{HCl}=1)$, i.e., the $HCl(v=1)+CHD_2(0_0)$ product pair from the ground-state reactants, clear forward-backward peaking distributions are seen in addition to the ridge structure. A closer inspection further unveils that the ridge structure here does not look like the above two for $(v_{HCl}=0)$ and $(v_{HCl}=0)^{\neq}$. We surmised that the ridge here actually comprises two overlapped ridges: a fast-evolving (with respect to collision energy) one with higher backward intensity at lower E_c, and as E_c increases, it merges into a slow-evolving one that is similar to the ones in the upper panel. The fast-evolving ridge near the energetic threshold, together with the forward-backward peaking dis-

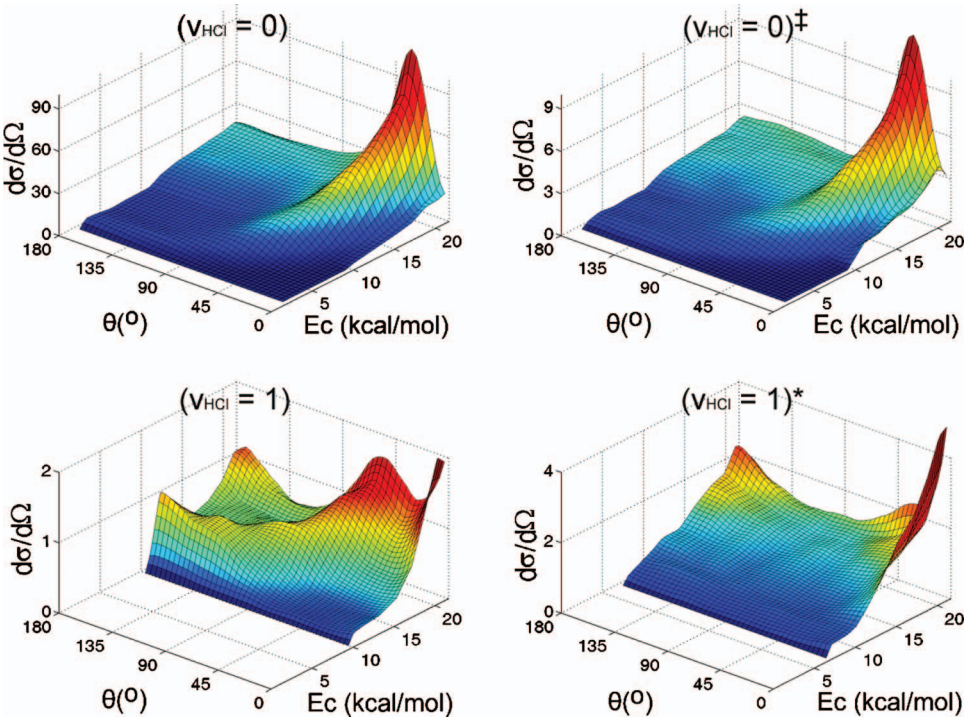

FIG. 9. (Color) Three-dimensional representations of $d\sigma/d\Omega$-θ-E_c that summarize the evolution of correlated angular distributions with collisional energies for reactions of $Cl+CH_2D_2 \rightarrow CHD_2(0_0)+HCl(v)$. Note the different intensity scales of each panel. The angular distributions are weighed by their respective populations of reactant states (i.e., similar to the left-top panel of Fig. 7). Distinct patterns are clearly seen, suggestive of two dominant underlying reaction pathways: a direct pathway evolving from the rebound mechanism at low E_c to a peripheral dynamics at high E_c for $(v_{HCl}=0)$ and $(v_{HCl}=0)^{\neq}$, and an additional resonant complex mechanism also contributes, leading to the product channels labeled as $(v_{HCl}=1)$ and $(v_{HCl}=1)^*$.

tribution at higher E_c, is reminiscent of the characteristic pattern for reactive resonance uncovered in the $F+HD \rightarrow HF+D$ reaction.[38–40] The physical origin of this resonance signature, namely, how a dynamical resonance gives rise to a fast-evolving ridge followed by forward-backward peaking angular distribution in bimolecular reaction, has been elucidated and, to a large extent, understood.[6,39–41] Based on pattern comparison, we assert that the formation of $(v_{HCl}=1)$ from the ground-state reactant invokes both the resonance and the direct peripheral reaction pathways, which is also what we concluded previously for forming $HCl(v=1)$ in reactions of $Cl+CH_4$ (Ref. 9) and CHD_3.[25] A recent quantum dynamics and quasiclassical trajectory study of $Cl+CH_4$ on a pseudotriatomic *ab initio* based surface also unveiled similar imprints of a Feshbach resonance for the production of $HCl(v=1)$ (Ref. 42) in support of our experimental suggestion.[9]

As to the spin-orbit excited reaction of $Cl^*(^2P_{1/2})+CH_2D_2 \rightarrow HCl(v=1)+CHD_2(0_0)$, labeled as $(v_{HCl}=1)^*$ in Fig. 9, the pattern is dominated by the forward-backward peaking, with the ridge structures (both the low-energy resonance ridge and the high-energy peripheral ridge) being nearly invisible. Adiabatically, the spin-orbit excited $Cl^*(^2P_{1/2})$ cannot react with methane at the energy range of this study. Thus, the formation of $(v_{HCl}=1)^*$ must proceed through an electronically nonadiabatic process. The general pattern shown in Fig. 9 is reminiscent of that for $F^*(^2P_{1/2})+HD \rightarrow HF(v=3)+D$,[43] which has been ascribed to a resonance-mediated (spin-orbit) nonadiabatic process. Based on the prior *ab initio* calculations of the Cl+ methane reactions[44–46] and the vibrationally adiabatic correlation scheme,[9,25,26] a dynamical well that correlates the reactant-pair $Cl(^2P_{3/2})+CH_2D_2(v_1=1)$ to the product-pair $HCl(v=1)+CHD_2(0_0)$ is anticipated. We speculate that the nonadiabatic deactivation from the spin-orbit excited $Cl^*(^2P_{1/2})+CH_2D_2$ to the ground $Cl(^2P_{3/2})+CH_2D_2$ surfaces in the entrance channel, which is a prerequisite for $Cl^*(^2P_{1/2})$ to be reactive, is likely accompanied by a simultaneous promotion of the CH_2-symmetric stretch $(v_1=1)$ of the CH_2D_2 reactant. Asymptotically, one quantum excitation of the v_1-mode requires ~8.5 kcal/mol, which is significantly larger than the spin-orbit energy of $Cl^*(^2P_{1/2})$, 2.52 kcal/mol. However, the *ab initio* calculations indicated that the vibrational frequency of the v_1-mode will decrease drastically upon the approach of the Cl atom due to the strong curvature coupling to the reaction coordinate,[44–46] which would narrow the energy gap between the two vibronic surfaces along the reaction coordinate, facilitating the suggested (vibrationally mediated) electronic surface hopping process. At sufficiently high E_c, it could then lead to the observed $HCl(v=1)+CHD_2(0_0)$ product pair through the reactive resonance supported by the dynamic well on the $(v_1=1)$ vibrationally adiabatic curve.

The qualitative interpretation given here is obviously tentative and does not exclude other lower frequency vibrational modes of CH_2D_2 that are much closer in resonance to the spin-orbit splitting of the Cl atom from participating in the electronically nonadiabatic dynamics. (In fact, as mentioned above, some bending/torsional motions of CH_2D_2 are Corialis coupled to the symmetric-stretching mode.) We merely wish to emphasize the essential role of the symmetric-stretching mode in facilitating the spin-orbit nonadiabatic transition in order to account for the distinct formation of the $HCl(v=1)+CHD_2(0_0)$ pair. More theoretical work is invited.

Similarly, Fig. 10 presents the result of the four product pairs observed in the CH_2D+DCl isotopic channel. Although the details are not quite the same as the CHD_2+HCl channel—for example, the formation of $(v_{DCl}=0)^{\neq}$ from the bend-excited reaction shows a pronounced direct swath[38,40] in the backward hemisphere, the gross features of the periph-

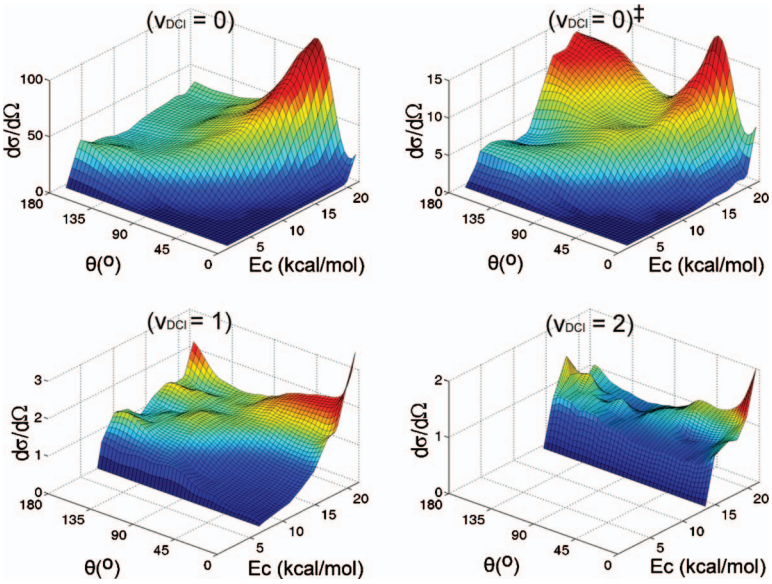

FIG. 10. (Color) Same as Fig. 9, but for reactions of $Cl+CH_2D_2 \rightarrow CH_2D(0_0)+DCl(v)$. Due to the beam background and image resolution problems, the results for spin-orbit excited reactivity cannot be obtained reliably over a wide range of energy; thus are not shown. The patterns indicate that the correlated ground-state DCl products, $(v_{DCl}=0)$ and $(v_{DCl}=0)^{\neq}$, are formed predominantly by direct rebound/peripheral reaction mechanisms, whereas the reactive resonance pathway also contributes to the formation of vibrationally excited DCl, that is, $(v_{DCl}=1)$ and $(v_{DCl}=2)$.

eral ridge (the upper panel) and the resonance characters (the lower panel) are retained. Hence, we assert that the formations of $(v_{DCl}=0)$ and $(v_{DCl}=0)^{\neq}$ are of direct reaction mechanism, whereas the productions of $(v_{DCl}=1)$ and $(v_{DCl}=2)$ proceed through both the direct and resonance pathways. Judging from the appearance, the formation of $DCl(v=2)+CH_2D(0_0)$ seems to be dominated more by the resonant reaction mechanism.

VII. CORRELATED ENERGY DISPOSAL

It is instructive to look back on a more average quantity, the correlated energy disposal of the two isotopic product channels from the dominant ground-state reaction, to gain further insights into their reactivity. The results for $Cl(^2P_{3/2})+CH_2D_2(v=0) \rightarrow HCl(v)+CHD_2(0_0)$ are summarized in Fig. 11. The fractional energy disposals are depicted in the upper panel and the absolute energy (in kcal/mol) are presented in the lower panel. Note the different scales on the right and left ordinates. Most of the available energy appears as product translational energy; moreover as E_c increases, the fractional kinetic energy release f_T remains nearly constant, ~88%. The remaining is largely deposited into HCl rotation, f_R. Note that the small HCl vibrational fraction f_V appears at the expense of HCl rotational degree of freedom.

Also shown as the heavy gray line in the lower panel is the prediction of the kinetic energy release E_T from the consideration of kinematic constraints.[8] The title reaction is essentially a heavy+light-heavy system, involving a H-atom transfer from the CHD_2 moiety to the attacking Cl atom. For such a mass combination of an endothermic reaction, a simple kinematics model predicts that the average kinetic energy release can be expressed as $E_T=(E_c-\Delta H_{rx})\cos^2\beta$.[47] Here, ΔH_{rx} is the endothermicity and β is the skew angle, $\cos^2\beta=m_A m_C/m_{AB}m_{BC}$, for the $A+BC \rightarrow AB+C$ reaction. The excellent agreement between the experimental data and the model prediction over such a wide range of E_c, in which no adjustable parameter is invoked, provides a compelling evidence for the dominant kinematics role in governing this attribute, as well the spectator nature of the methyl moiety in the ground-state reaction. This conclusion reinforces our previous findings for the $Cl+CH_4/CD_4$ (Ref 8) and $Cl+CHD_3$ reactions.[10]

Figure 12 presents similar analysis for the $DCl+CH_2D$

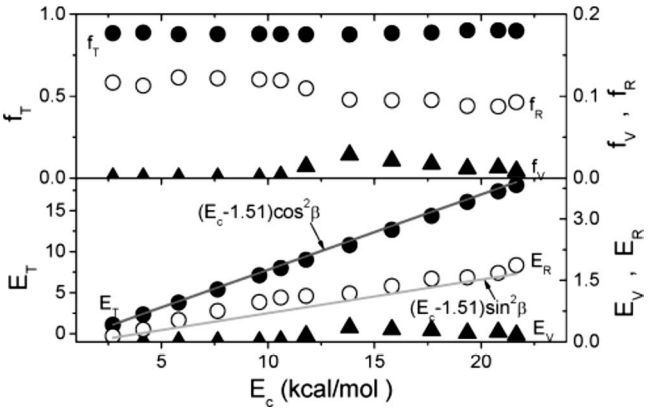

FIG. 11. Correlated energy disposal of the $Cl+CH_2D_2(0_0) \rightarrow CHD_2(0_0)+HCl(v)$ reaction. The fractional energy disposal is presented in the upper panel, and the energy disposal (in kcal/mol) in the lower panel. Note the different scales of the right and left ordinates. Predictions from a simple kinematics model are given by the gray lines.

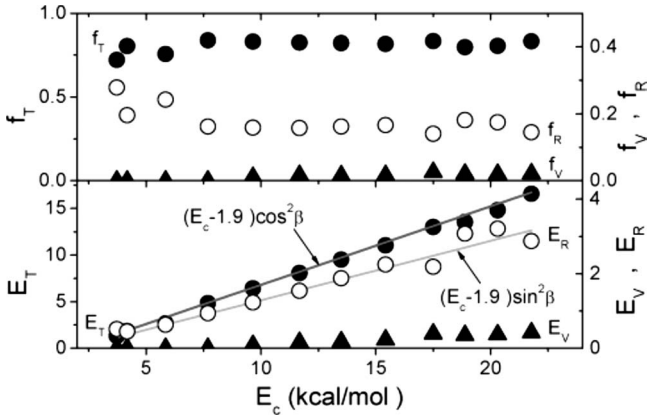

FIG. 12. Same as Fig. 11, but for the $Cl+CH_2D_2(0_0) \rightarrow CH_2D(0_0)+DCl(v)$ reaction.

isotope channel. Once again, the simple kinematics model accounts for the results remarkably well. A closer comparison between the two isotope channels reveals that the average kinetic energy release E_T for the H-atom abstraction channel is slightly larger than that for the D-atom channel. Alternatively, this may be more apparent from the comparison of the HCl/DCl rotational energy release, E_R. As discussed above, the reaction is mainly vibrationally adiabatic in the sense that the vibrational ground-state reactants yield mostly the vibrational ground-state products. Hence, the remaining energy release from the kinematics model, $(E_c - \Delta H_{rx})\sin^2\beta$, is mainly deposited into the HCl/DCl rotation. Indeed, this is what we observed, as shown by the thin gray lines in Figs. 11 and 12. For the two isotopic channels, E_R(DCl) is about twice larger than E_R(HCl); for example, at $E_c=20$ kcal/mol E_R(HCl) and E_R(DCl) are 1.5 and 2.8 kcal/mol, respectively. For a $A+BC$ reaction, the angular momentum disposal can be expressed as $\boldsymbol{j}'=\boldsymbol{l}\sin^2\beta+\boldsymbol{j}\cos^2\beta+\boldsymbol{d}\cos^2\beta$.[47] Here, $\boldsymbol{j}'(\boldsymbol{j})$ is the product (reactant) rotational angular momentum (we neglected the low-N angular momenta of the probed methyl products, which were kept the same for all E_c in this study), $\boldsymbol{l}$ is the initial orbital angular momentum of the colliding reactants, and $\boldsymbol{d}$ is a transformation vector incorporating the effect of reaction dynamics.[47] Since $\boldsymbol{j}\approx 0$ for a supersonic CH_2D_2 beam and, as just shown, the kinematics dominates the energy disposal, we conjectured that the dynamical factor $\boldsymbol{d}$ is also small. In other words, we approximated $\boldsymbol{j}'\approx\boldsymbol{l}\sin^2\beta=0.081\boldsymbol{l}$ (or $0.16\boldsymbol{l}$) for the HCl (or DCl) channel. The rotational constants for HCl and DCl are 10.44 and 5.4 cm^{-1}, respectively. From the average rotational energies E_R given above, one has $j'_{HCl}\approx 7\hbar$ and $j'_{DCl}\approx 13\hbar$, which, in turn, lead to $l\sim 86\hbar$ and $81\hbar$ for the HCl and DCl channels, respectively, at $E_c\sim 20$ kcal/mol.

The estimated l-values here refer to the average orbital angular momentum of the two reactants. Because the reaction is of the peripheral type, the opacity function strongly favors larger l. Hence, the average value of l should be quite close to the peak-l of the opacity function, which is in reasonable accord with theoretical results for the isotopically analogous reactions.[3,10,48,49] Moreover, the closeness of the two l-values estimated for the HCl and DCl channels implies that the respective reactive cross sections cannot be very different. From Figs. 7 and 8 (left-top panels), the measured cross sections, without accounting for the detection sensitivity differences when probing the low N-states of $CHD_2(0_0^0)$ and $CH_2D(0_0^0)$, are nearly the same. It then suggests that the (2+1) REMPI detections of the two isotopic methyl radicals may have approximately the same sensitivity—a point needs future confirmation.

VIII. CONCLUSIONS

In this report, we focus on the correlated reaction dynamics associated with the ground state of methyl radicals $CHD_2(0_0)$ and $CH_2D(0_0)$, which are the major products of the title reaction. Thanks to the high resolution of the time-sliced velocity-imaging detection scheme, the raw images revealed the coincidently formed HCl/DCl coproducts in a state-resolved manner from not only the ground-state reactants but also the bend-excited CH_2D_2 and the spin-orbit excited $Cl^*(^2P_{1/2})$ reactants. In other words, state-to-state correlated dynamics for three different combinations of reactant pairs, i.e., $Cl(^2P_{3/2})+CH_2D_2(0_0)$, $Cl(^2P_{3/2})+CH_2D_2(v_{bend}=1)^{\neq}$, and $Cl^*(^2P_{1/2})+CH_2D_2(0_0)$, were acquired simultaneously by imaging the $CHD_2(0_0)$ and $CH_2D(0_0)$ products. The relative reactivity of the observed eight different product-pair channels were characterized, where possible, and their dynamical attributes were elucidated. Two distinct reaction mechanisms, direct peripheral and reactive resonance, were put forward to account for the observations. Similar isotope effects as those found previously in $Cl+CH_4/CD_4$ and $Cl+CHD_3$ were also observed, which appear to be a universal trait of this benchmark reaction of chlorine atom+methane.

ACKNOWLEDGMENTS

We are indebted to S. Yan and H. Y. Liao for their helps in experiments. This work was financially supported by National Science of Council of Taiwan, Academia Sinica, and the (U.S.) Air Force Office of Scientific Research (Grant No. AOARD-07-4005).

[1] S. Solomon, Rev. Geophys. **37**, 275 (1999).
[2] H. A. Michelsen, Acc. Chem. Res. **34**, 331 (2001), and references therein.
[3] D. Troya, J. Millan, I. Banos, and M. Gonzalez, J. Chem. Phys. **117**, 5730 (2002), and references therein.
[4] R. N. Zare, Science **279**, 1875 (1998).
[5] F. F. Crim, Acc. Chem. Res. **32**, 877 (1999).
[6] K. Liu, Annu. Rev. Phys. Chem. **52**, 139 (2001); J. Chem. Phys. **125**, 132307 (2006).
[7] X. Wang, M. Ben-Nun, and R. D. Levine, Chem. Phys. **197**, 1 (1995).
[8] J. Zhou, B. Zhang, J. J. Lin, and K. Liu, Mol. Phys. **103**, 1757 (2005).
[9] B. Zhang and K. Liu, J. Chem. Phys. **122**, 101102 (2005).
[10] G. Nyman, J. Zhou, B. Zhang, and K. Liu, Isr. J. Chem. **47**, 1 (2007).
[11] G. Nyman, D. C. Clary, and R. D. Levine, Chem. Phys. **191**, 223 (1995).
[12] Z. H. Kim, H. A. Bechtel, and R. N. Zare, J. Am. Chem. Soc. **123**, 12714 (2001).
[13] H. A. Bechtel, Z. H. Kim, J. P. Camden, and R. N. Zare, J. Chem. Phys. **120**, 791 (2004).
[14] J. Riedel, S. Yan, H. Kawamata, and K. Liu, Rev. Sci. Instrum. **79**, 033105 (2008).
[15] J. J. Lin, J. Zhou, W. Shiu, and K. Liu, Rev. Sci. Instrum. **74**, 2495 (2003).
[16] U. Even, J. Jortner, D. Noy, and N. Lavie, J. Chem. Phys. **112**, 8068 (2000).
[17] J. L. Brum, R. D. Johnson III, and J. W. Hudgens, J. Chem. Phys. **98**, 3732 (1993).
[18] B. Zhang, S. Yan, and K. Liu, J. Phys. Chem. A **111**, 9263 (2007).
[19] K. Liu, Phys. Chem. Chem. Phys. **9**, 17 (2007).
[20] J. Zhou, W. Shiu, J. J. Lin, and K. Liu, J. Chem. Phys. **120**, 5863 (2004); **124**, 104309 (2006).
[21] S. Yan and K. Liu, Chin. J. Chem. Phys. **20**, 333 (2007).
[22] W. Shiu, J. J. Lin, K. Liu, M. Wu, and D. H. Parker, J. Chem. Phys. **120**, 117 (2004).
[23] D. M. Sonnenfroh and K. Liu, Chem. Phys. Lett. **176**, 183 (1991).
[24] J. Zhou, J. J. Lin, B. Zhang, and K. Liu, J. Phys. Chem. A **108**, 7832 (2004).
[25] S. Yan, Y.-T. Wu, B. Zhang, X.-F. Yue, and K. Liu, Science **316**, 1723 (2007).
[26] S. Yan, Y.-T. Wu, and K. Liu, Proc. Natl. Acad. Sci. U.S.A. **105** 12667 (2008).
[27] J. J. Lin, J. Zhou, W. Shiu, and K. Liu, Science **300**, 966 (2003).
[28] J. Zhou, J. J. Lin, W. Shiu, and K. Liu, J. Chem. Phys. **119**, 4997 (2003).
[29] S. C. Althorpe, F. Fernandez-Alonso, B. D. Bean, J. D. Ayers, A. E. Pomerantz, R. N. Zare, and E. Wrede, Nature (London) **416**, 67 (2002).

[30] S. A. Harich, D. Dai, C. C. Wang, X. Yang, S. D. Chao, and R. T. Skodje, Nature (London) **419**, 281 (2002).
[31] D. E. Manolopoulos, Nature (London) **419**, 266 (2002).
[32] J. L. Duncan and M. M. Law, Spectrochim. Acta, Part A **53**, 1445 (1997).
[33] B. Zhang and K. Liu, J. Phys. Chem. A **109**, 6791 (2005).
[34] H. A. Bechtel, J. P. Camden, D. J. A. Brown, M. R. Martin, R. N. Zare, and K. Vodopyanov, Angew. Chem., Int. Ed. **44**, 2382 (2005).
[35] B. Retail, J. K. Pearce, C. Murray, and A. J. Orr-Ewing, J. Chem. Phys. **122**, 101101 (2005).
[36] B. Retail, S. J. Greaves, J. K. Pearce, R. A. Rose, and A. J. Orr-Ewing, Phys. Chem. Chem. Phys. **9**, 3261 (2007).
[37] B. Retail, J. K. Pearce, S. J. Greaves, R. A. Rose, and A. J. Orr-Ewing, J. Chem. Phys. **128**, 184303 (2008).
[38] R. T. Skodje, D. Skouteris, D. E. Manolopoulos, S.-H. Lee, F. Dong, and K. Liu, Phys. Rev. Lett. **85**, 1206 (2000).
[39] S.-H. Lee, F. Dong, and K. Liu, J. Chem. Phys. **116**, 7839 (2002).
[40] S.-H. Lee, F. Dong, and K. Liu, J. Chem. Phys. **125**, 133106 (2006).
[41] K. Liu, R. T. Skodje, and D. E. Manolopoulos, PhysChemComm **5**, 27 (2002).
[42] R. Martínez, M. Gonzalez, P. Defazio, and C. Petrongolo, J. Chem. Phys. **127**, 104302 (2007).
[43] S.-H. Lee, F. Dong, and K. Liu, Faraday Discuss. **127**, 49 (2004).
[44] W. T. Duncan and T. N. Truong, J. Chem. Phys. **103**, 9642 (1995).
[45] J. C. Corchado, D. G. Truhlar, and J. Espinosa-Garcia, J. Chem. Phys. **112**, 9375 (2000).
[46] S. Yoon, R. J. Holiday, E. L. Sibert III, and F. F. Crim, J. Chem. Phys. **119**, 9568 (2003).
[47] R. D. Levine and R. B. Bernstein, *Molecular Reaction Dynamics and Chemical Reactivity* (Oxford University Press, Oxford, 1987).
[48] H.-G. Yu and G. Nyman, Phys. Chem. Chem. Phys. **1**, 1181 (1999).
[49] D. Troya and P. J. E. Weiss, J. Chem. Phys. **124**, 074313 (2006).